AD-A145 636 NEUTRAL BEAM INTERACTIONS WITH MATERIALS(U) MICHIGAN 1/1
UNIV ANN ARBOR PARTICLE BEAM RESEARCH LAB
R S ONG ET AL. JUN 84 AFOSR-TR-84-0690 AFOSR-80-0029
UNCLASSIFIED F/G 20/9 NL

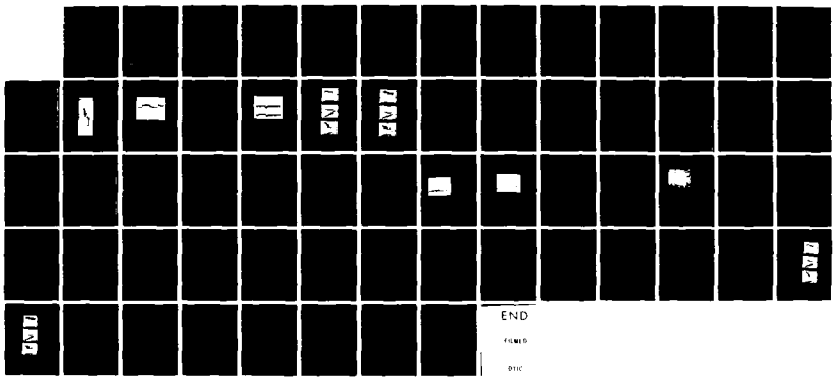

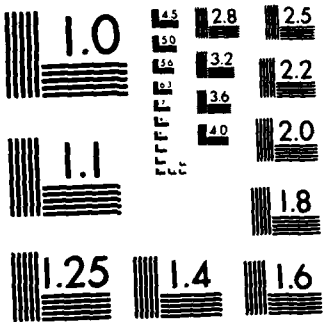

AFOSR-TR- 0690

(5)

AD-A145 636

Annual Progress Report to:
The Air Force Office of Scientific Research
for the Project:

Neutral Beam Interactions with Materials AFOSR 80-0029

Period: June 1, 1983 - May 31, 1984

R.S. Ong
Aerospace Eng. Dept.

J.J. Duderstadt
Nuclear Eng. Dept. and
Dean, College of Engineering

R.M. Gilgenbach
Nuclear Engineering Dept.

DTIC FILE COPY

Particle Beam Research Laboratory
June 1984

Unclassified

SECURITY CLASSIFICATION OF THIS PAGE (When Data Entered)

REPORT DOCUMENTATION PAGE		READ INSTRUCTIONS BEFORE COMPLETING FORM
1. REPORT NUMBER AFOSR-TR- 84-0990	2. GOVT ACCESSION NO. AD-A145636	3. RECIPIENT'S CATALOG NUMBER
4. TITLE (and Subtitle) Neutral Beam Interactions with Materials		5. TYPE OF REPORT & PERIOD COVERED Annual Report
		6. PERFORMING ORG. REPORT NUMBER
7. AUTHOR(s) R. M. Gilgenbach, R. S. Ong, and J. J. Duderstadt		8. CONTRACT OR GRANT NUMBER(s) AFOSR 80-0029
9. PERFORMING ORGANIZATION NAME AND ADDRESS The University of Michigan Ann Arbor, MI 48109		10. PROGRAM ELEMENT, PROJECT, TASK AREA & WORK UNIT NUMBERS 2301/A7 PE61102F
11. CONTROLLING OFFICE NAME AND ADDRESS Air Force Office of Scientific Research Bolling AFB, Washington D.C. 20332		12. REPORT DATE June 1984
		13. NUMBER OF PAGES 58
14. MONITORING AGENCY NAME & ADDRESS(if different from Controlling Office)		15. SECURITY CLASS. (of this report) Unclassified
		15a. DECLASSIFICATION/DOWNGRADING SCHEDULE

16. DISTRIBUTION STATEMENT (of this Report)

Approved for public release; distribution unlimited.

17. DISTRIBUTION STATEMENT (of the abstract entered in Block 20, if different from Report)

18. SUPPLEMENTARY NOTES

19. KEY WORDS (Continue on reverse side if necessary and identify by block number)

Neutral beam, solid target material, duopigatron ion source, ion source plasma stability, intermediate and heavy beams, geometric focusing, displaced aperture focusing, stopping power, radiation field.

20. ABSTRACT (Continue on reverse side if necessary and identify by block number)

A duopigatron has been used to accelerate ion and neutral beams of hydrogen, argon, krypton, and xenon. An important class of ion source plasma instabilities has been investigated. The frequency of source plasma oscillations scale as the square root of ion mass. Ion extraction efficiencies for the various mass species show excellent agreement with theory in the transition

DD FORM 1 JAN 73 1473 EDITION OF 1 NOV 65 IS OBSOLETE

S/N 0102-LF-014-6601

Unclassified

SECURITY CLASSIFICATION OF THIS PAGE (When Data Entered)

from the space charge limited regime to the ion saturation regime. Displaced aperture grids with geometric focusing have been studied. Ruby laser ablation plasma experiments are underway and the ablation plasma parameters have been measured. Theoretical research has been directed towards developing analytic expressions for neutral beam stopping in solid matter in order to compare with ion beam stopping. A second part of the theoretical effort concerns coupling of three computational physics models to simulate the interaction between a neutral/ion beam with a target ablation plasma.

Table of Contents

I Experimental Program

Ia) Experimental Configuration

The duopigatron ion/neutral beam experiment has been significantly upgraded during the past year. An overall view of the experiment is presented in figure 1. A number of source plasma probes have been installed within the duopigatron in order to investigate the stability of high density source plasmas. These probes are depicted in figure 2. Reproducibility of the duopigatron has been improved with the development of an automatic digital sequence control system. The arc and beam control circuitry is shown schematically in figure 3. Optical couplers have been employed to isolate the high voltage sections from the sequence controller. Modifications of the high voltage ignitron switching and crowbarring system (Fig. 4) have included the addition of series inductance in order to slow the current rise to prevent spurious crowbarring at higher voltages. A frequency modulated fiber optic data link was developed in order to measure arc currents while the ion source is at high voltage.

Ib) Source Plasma Stability Experiments

One of the most significant discoveries in the course of this research has been a new class of source plasma instabilities which occur under certain conditions of arc

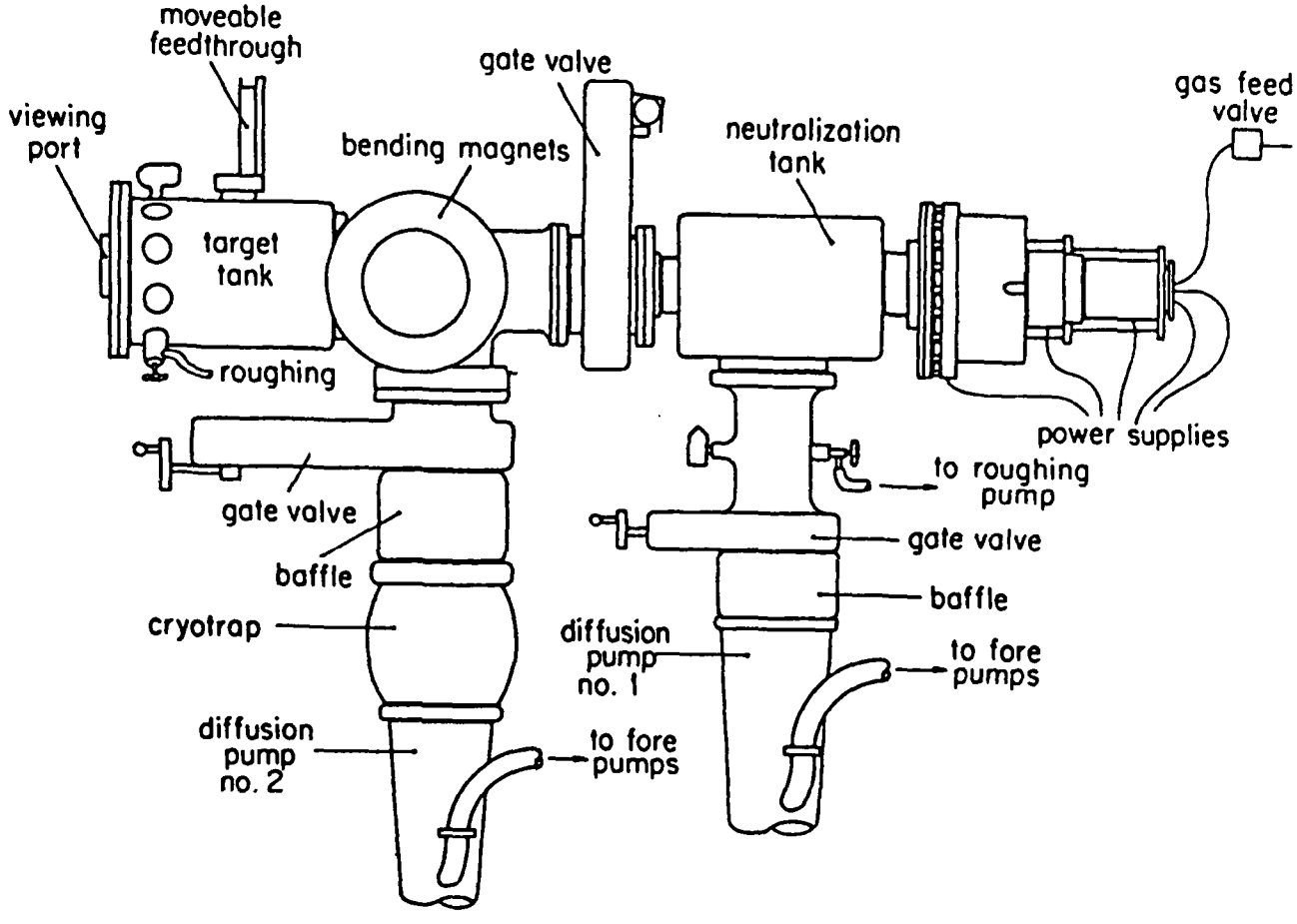

Figure 1. **Beamline, showing source, neutralization tank, target tank, and vacuum systems.**

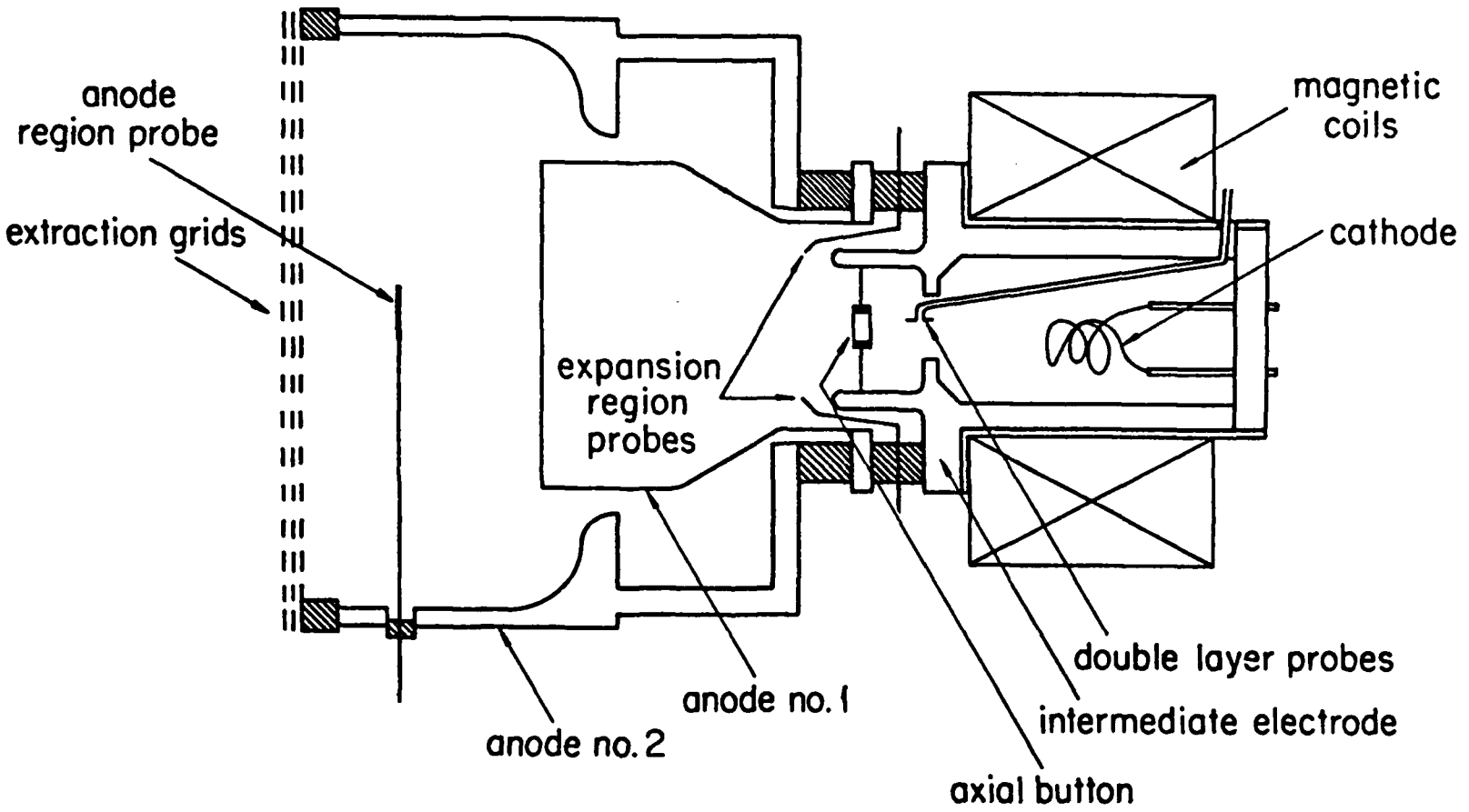

Figure 2. Cross-section of 10 cm Duopigatron.

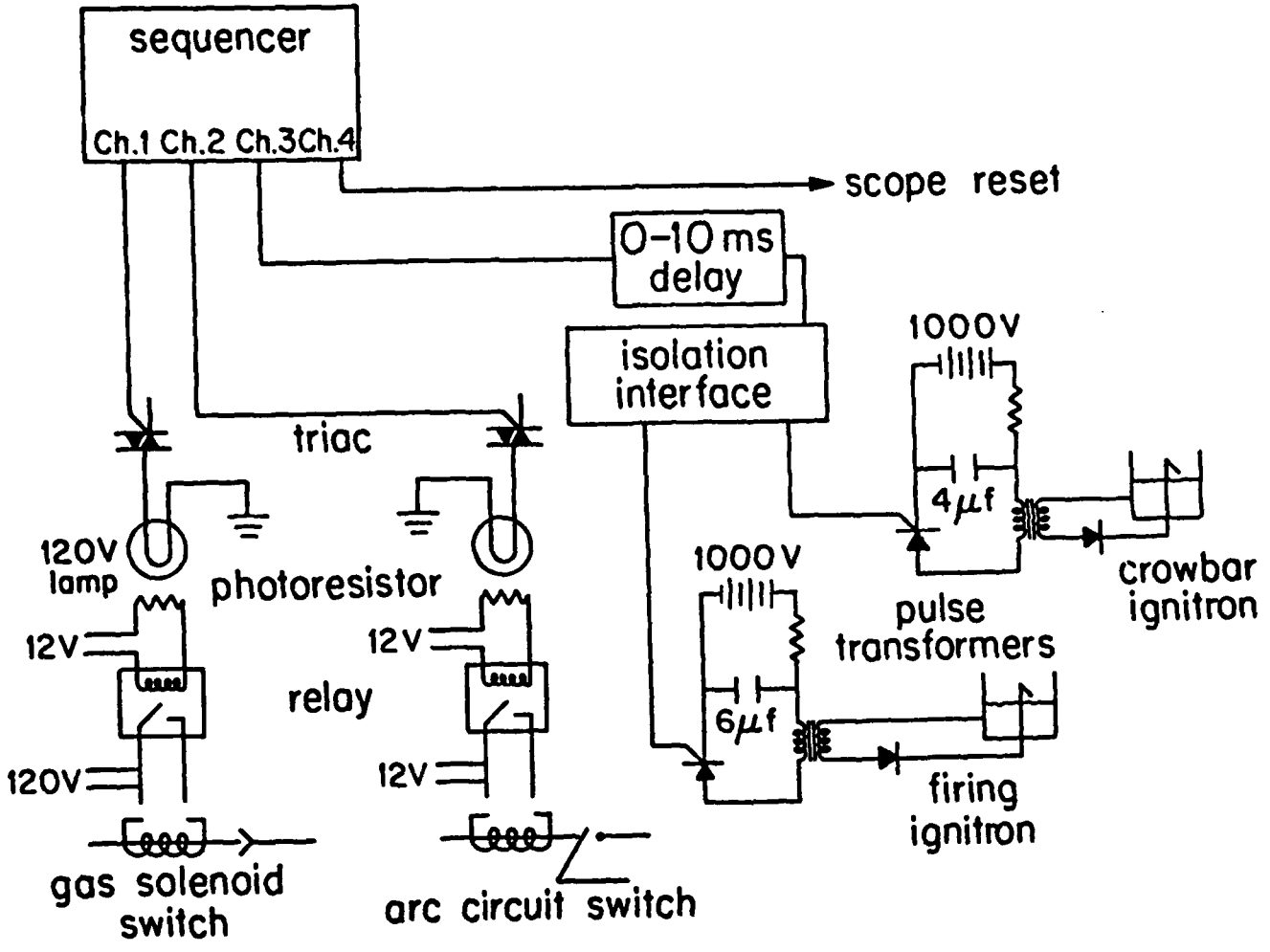

Figure 3. Arc and beam control circuitry.

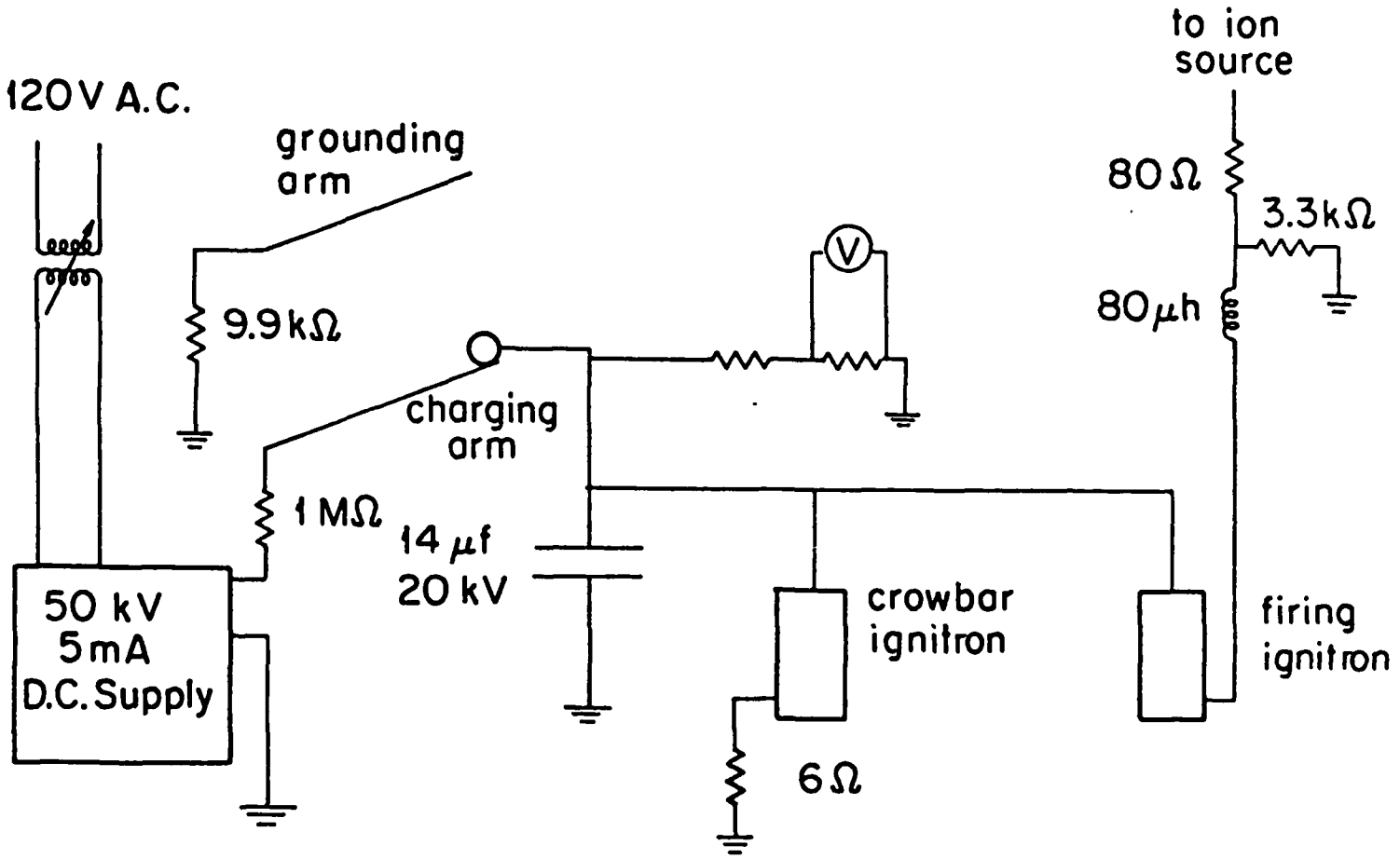

Figure 4. Schematic of capacitive discharge beam power supply.

current and gas pressure. This instability was studied primarily for intermediate and high mass gases, however, the mechanism is quite general and could also occur in hydrogen. Figure 5 shows the voltage versus current characteristics of the duopigatron source with argon fill gas. Note the large drop in arc voltage (Δ V) which occurs with increasing current around 13 A arc current. Langmuir probe data taken for krypton (figure 6) yield an electron temperature of about 1.4 eV with an electron density of about 5×10^{11} cm^{-3}. These source plasma data agree quite well with the results of a finite element computer code "DIST" as can be seen from figure 6b.

The mode shift fluctuations shown in the oscilloscope photograph of Figures 7 and 8 exhibited amplitudes of 30% to 80% of the arc current. Other investigators have speculated that these oscillations are due to E X B rotational instabilities, however, the magnetic field dependence of the oscillation frequency (figure 9) does not support their hypothesis. The data of Figure 9 does, in fact, show close agreement with an ion accoustic mass scaling ($M^{1/2}$). We performed other experiments using two azimuthally separated probes in order to identify whether rotational motion was occurring in the source plasma. These results shown in Figure 10 did not reveal any significant phase shifts. The data of Figures 11 and 12 clearly indicate the dual

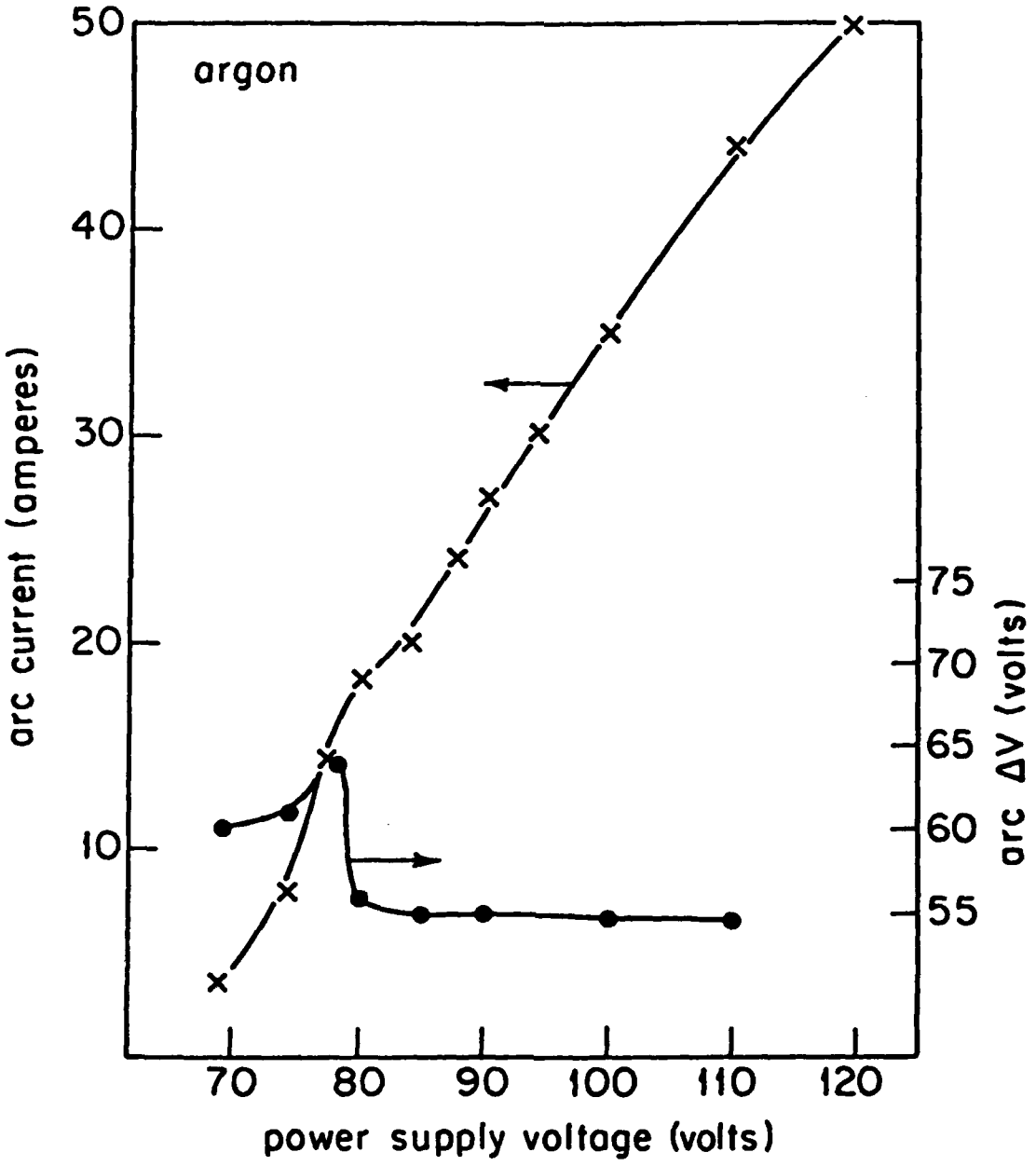

Figure 5. Argon arc current and arc voltage drop as a function of arc power supply voltage.

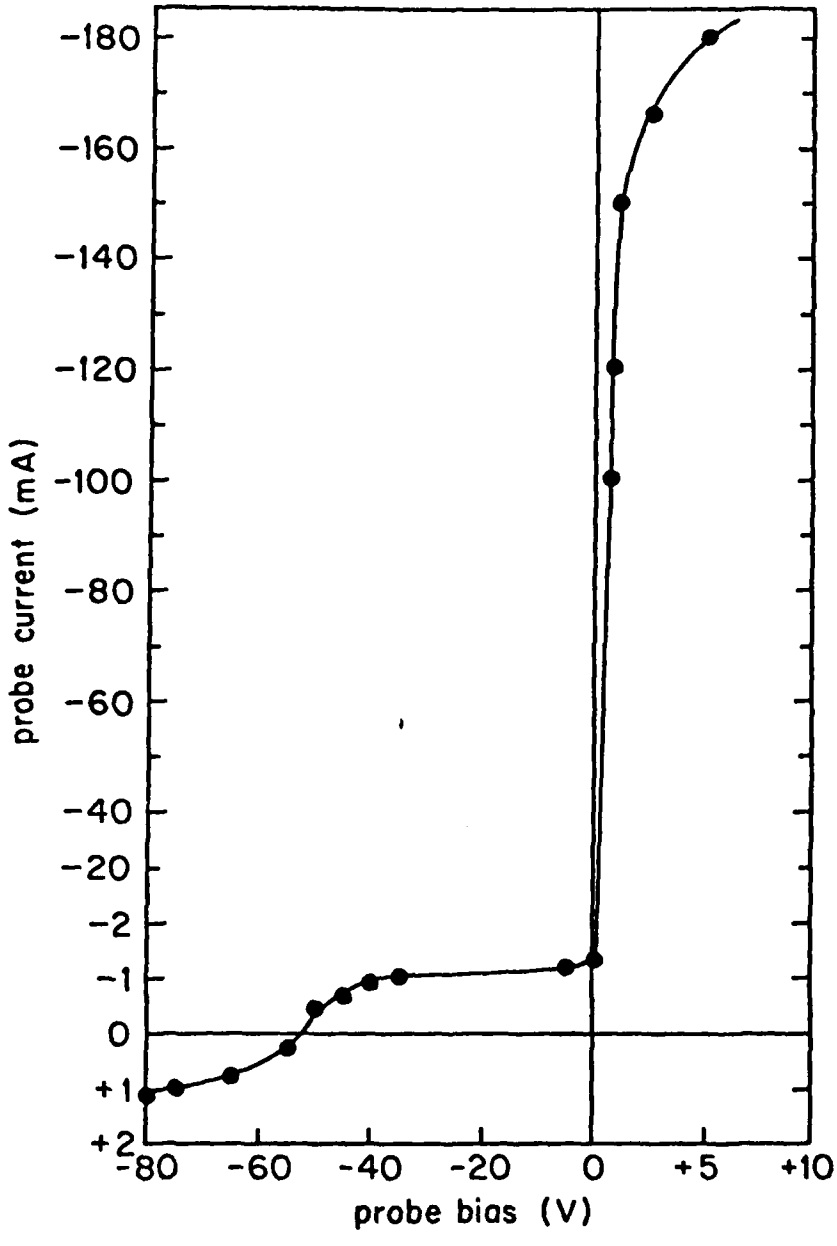

Figure 6. **Krypton source plasma Langmuir probe characteristic curve, at source centerline.**

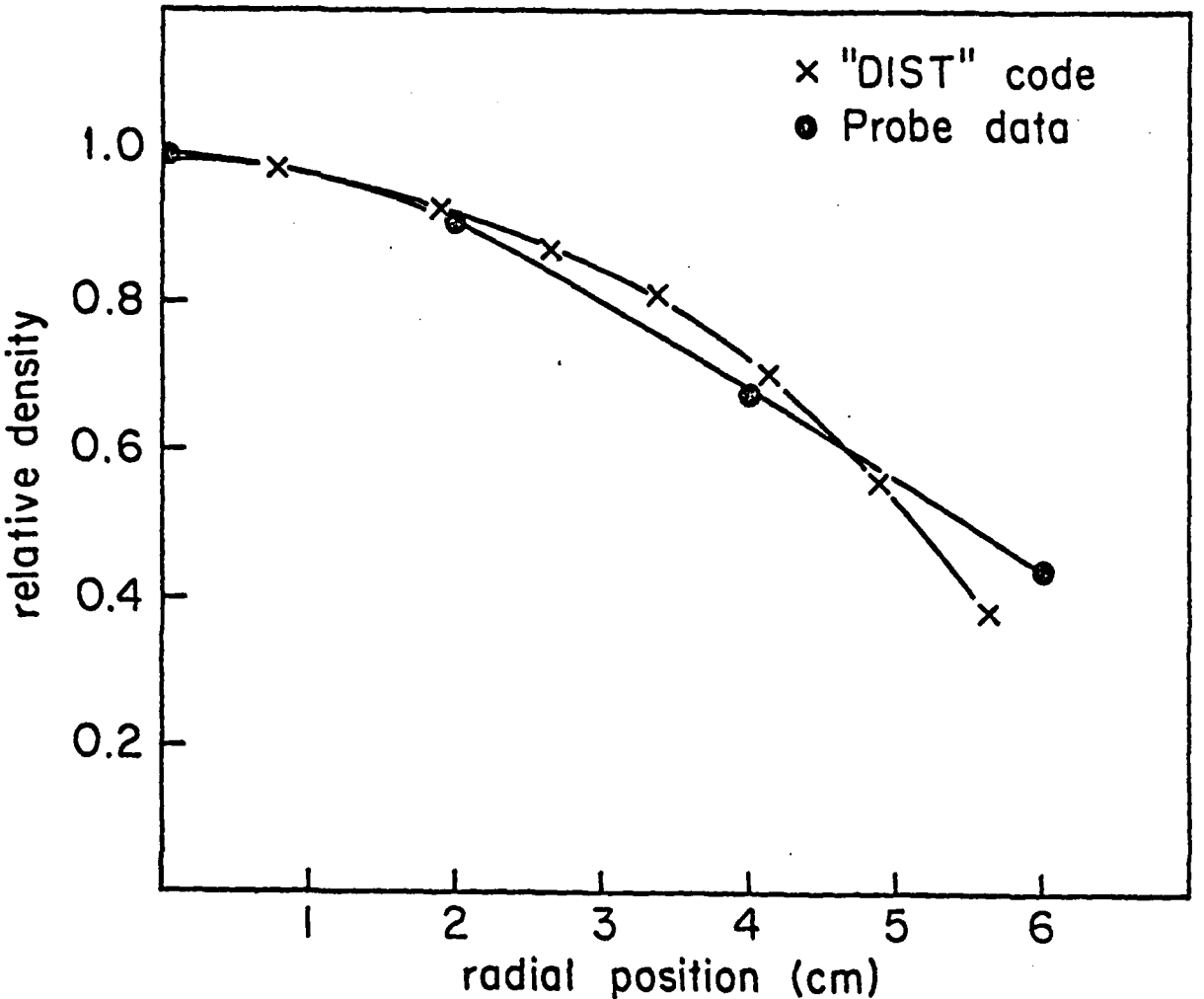

Fig. 6b Source plasma radial density distribution for 8 ampere argon arc, from moveable probe data, and "DIST" finite element code.

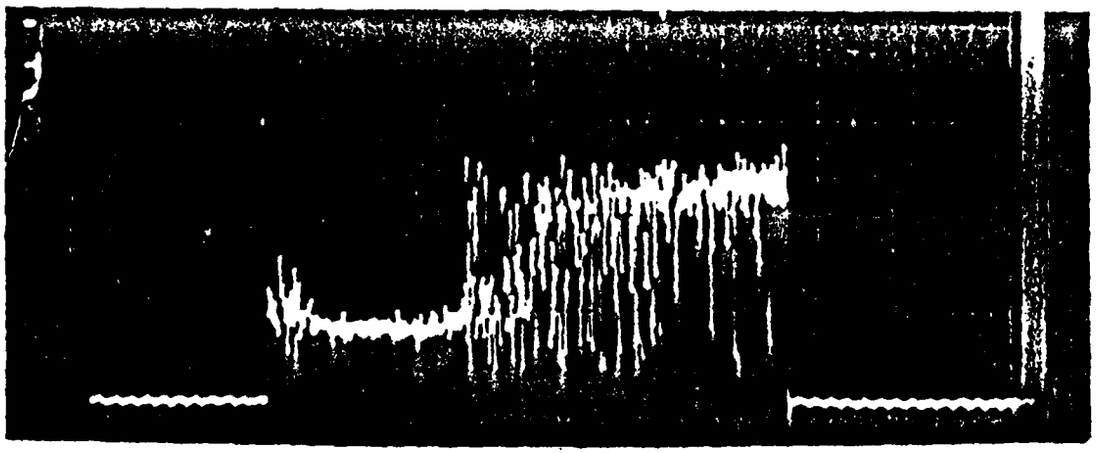

Figure 7. Illustration of mode shift fluctuation in argon (4 A/div., 200 msec/div.)

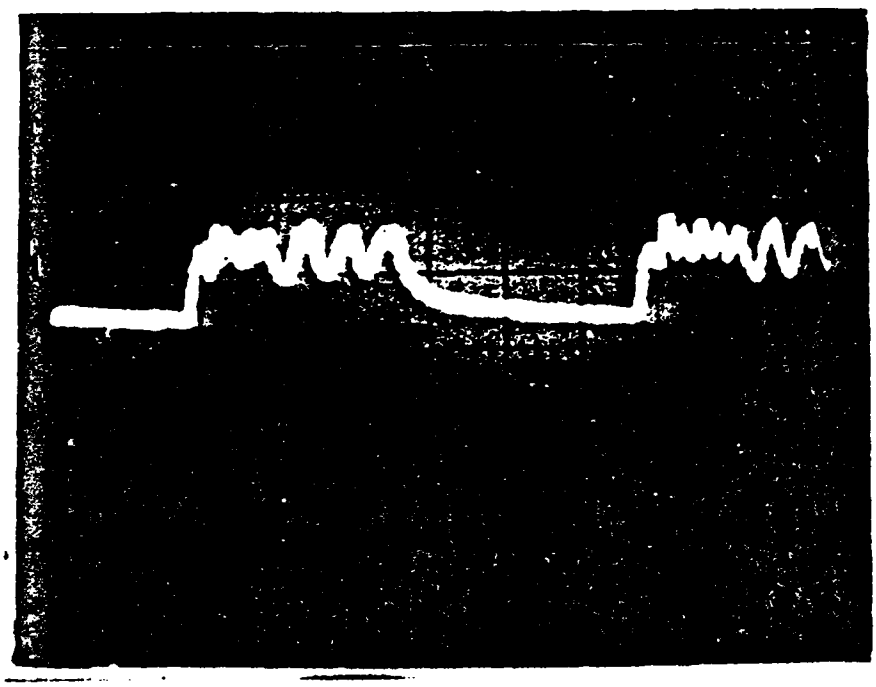

Figure 8. **Rapid structure of mode shift fluctuation in xenon (4 A/div., 0.2 msec/div.)**

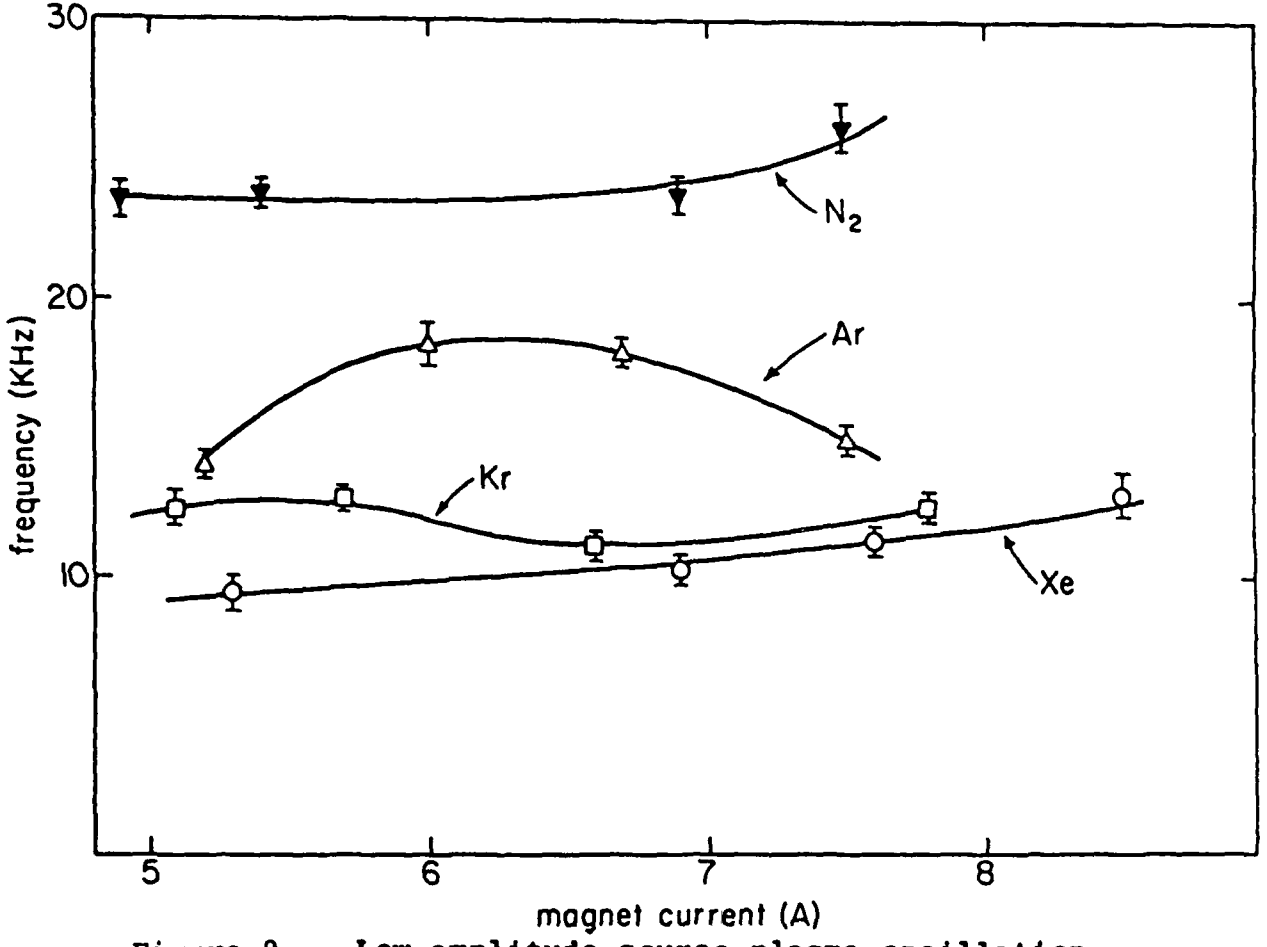

Figure 9. **Low amplitude source plasma oscillation frequency as a function of source magnet current.**

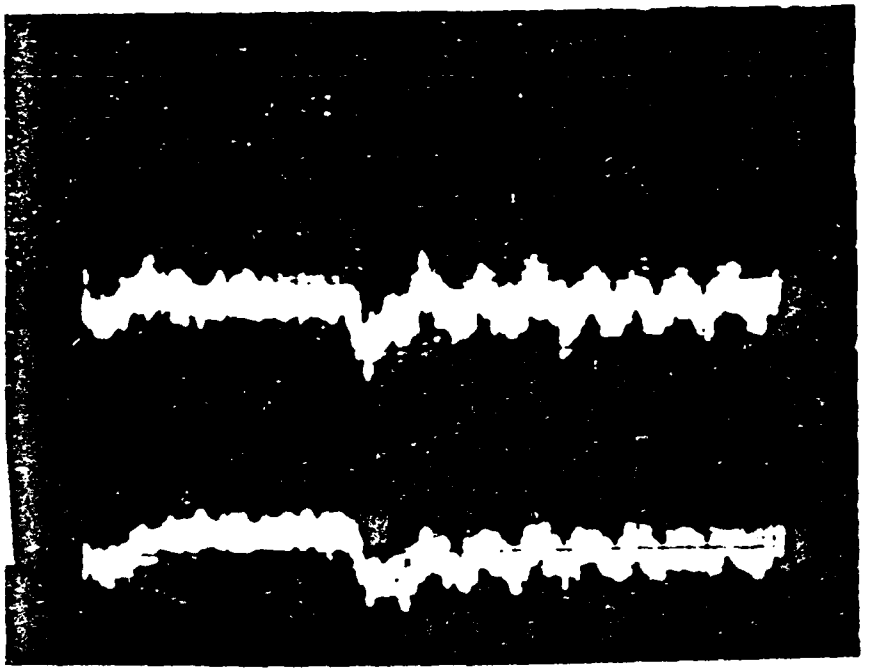

Figure 10. **Test for possible phase shift between two anode region probes, measuring electron saturation current.(45 mA/div., 0.1 msec/div.)**

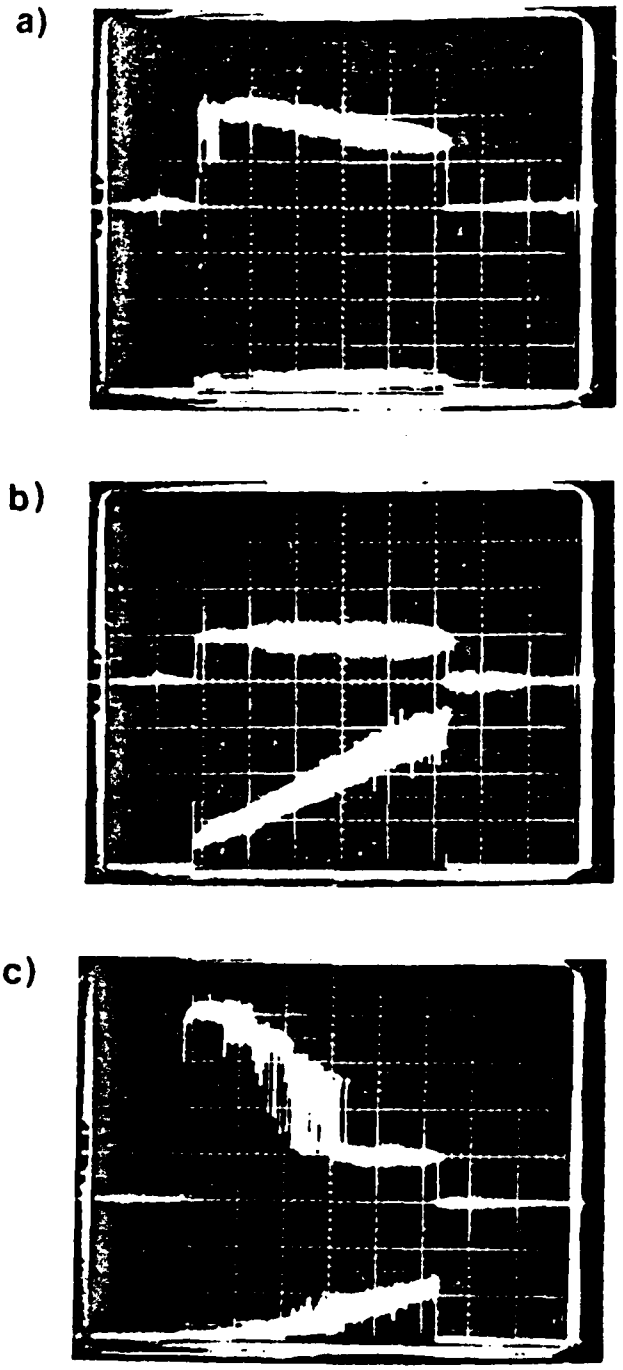

Figure 11. Arc current (lower trace, 4 A/div.) and double layer probe potential difference (upper trace, 10 V/div.) for argon in a) low current mode, b) high current mode, and c) mode shift regime. (200 msec/div.)

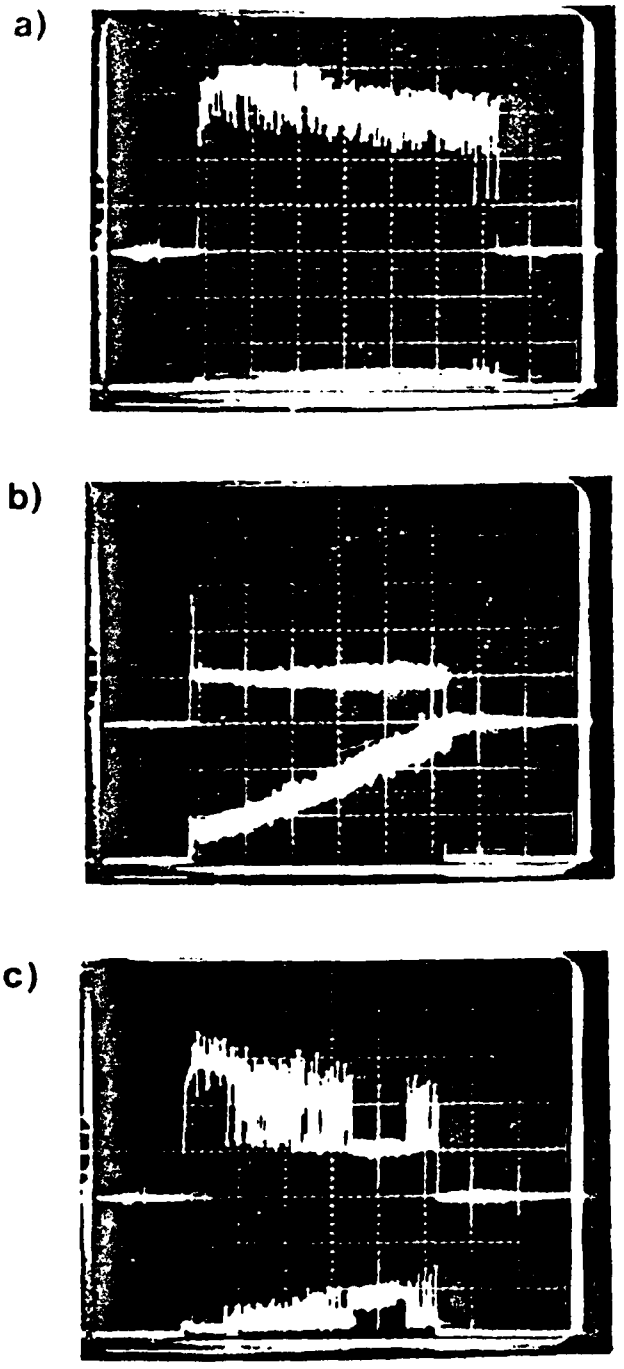

Figure 12. Arc current (lower trace, 4 A/div.) and double layer probe potential difference (upper trace, 10 V/div.) for krypton in a)low current mode, b) high current mode, and c) mode shift regime. (200 msec/div.)

mode characteristics of source plasma as indicated by the arc current and double layer potential difference. In the low current discharges we found that the floating potential was large while in the high current case the potential difference was much smaller. Detailed studies of this effect performed in a doctoral dissertation by P. W. Weber have shown that this instability is related to fluctuations in the double layer which are transmitted to the bulk source plasma by streaming electrons.

I c) Acceleration of Intermediate and High Mass Beams from a Duopigatron

An extensive series of experiments were performed to investigate the extraction and acceleration of intermediate and high mass ion beams from a duopigatron. The results of figures 13, 14, 15, and 16 show that the duopigatron is an efficient ion source over a wide range of masses. These data have improved the physical understanding of ion optics and focusing in the extraction grid of high current accelerators. Note that in each case the ion beam current reaches a plateau near the voltage labeled V^*. This voltage is defined as the voltage at which the ion saturation current from the source plasma is equal to the Child-Langmuir current:

$$V^* = \left[9 j_+ d^2 / 4\epsilon_0 (2e)^{\frac{1}{2}}\right]^{2/3} M^{1/3}$$

Note that V^* is a function of the grid spacing as well as

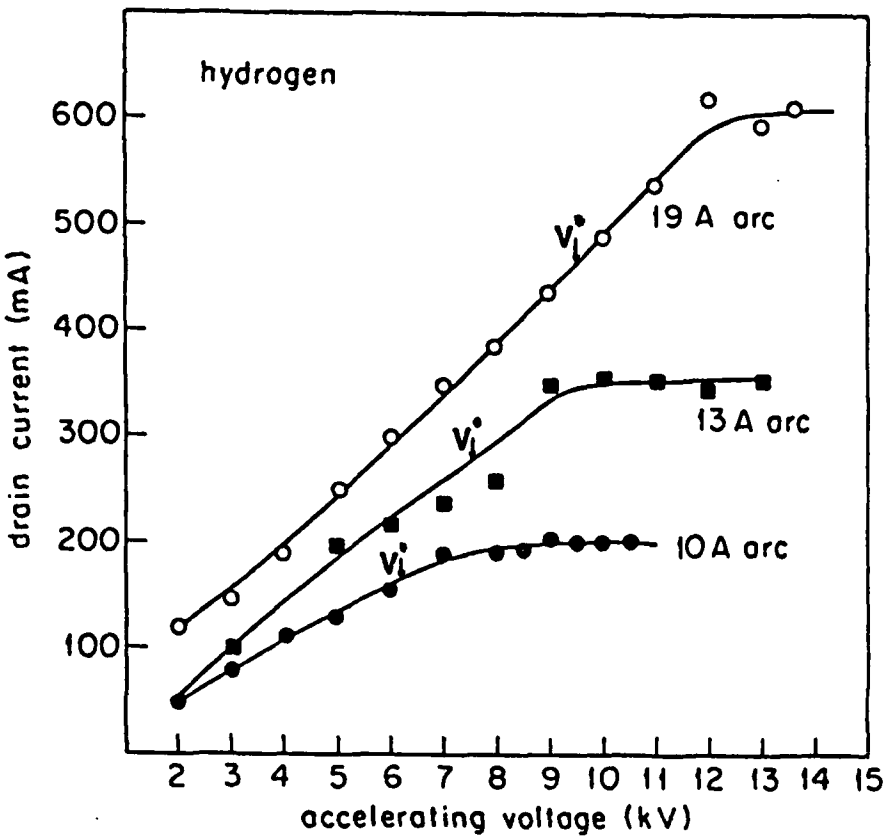

Figure 13. **Hydrogen beam drain current for 11 A, 13 A, and 19 A arc discharges.**

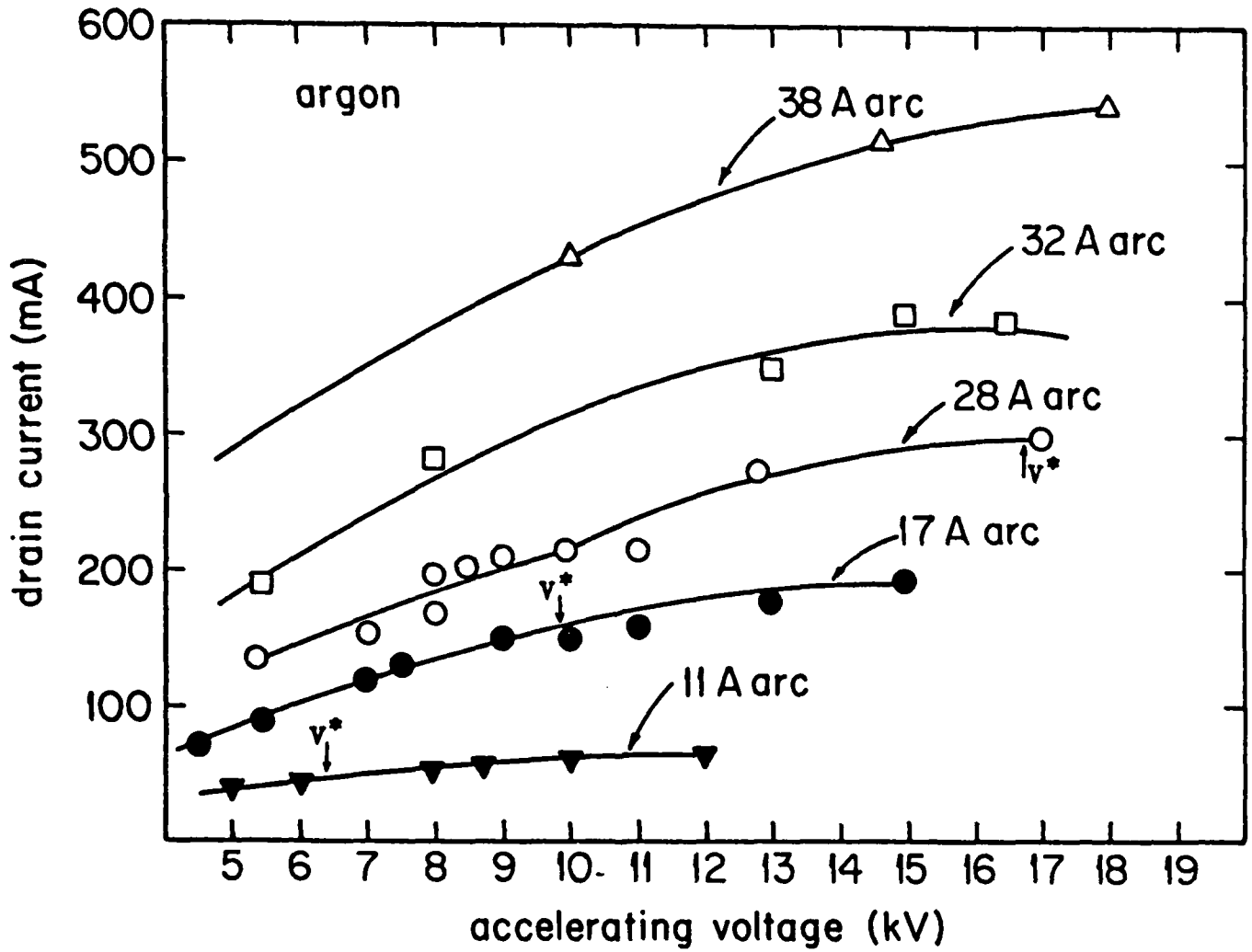

Figure 14. **Argon beam drain current for 11 A, 17 A, 28 A, 32 A, and 38 A arc discharges.**

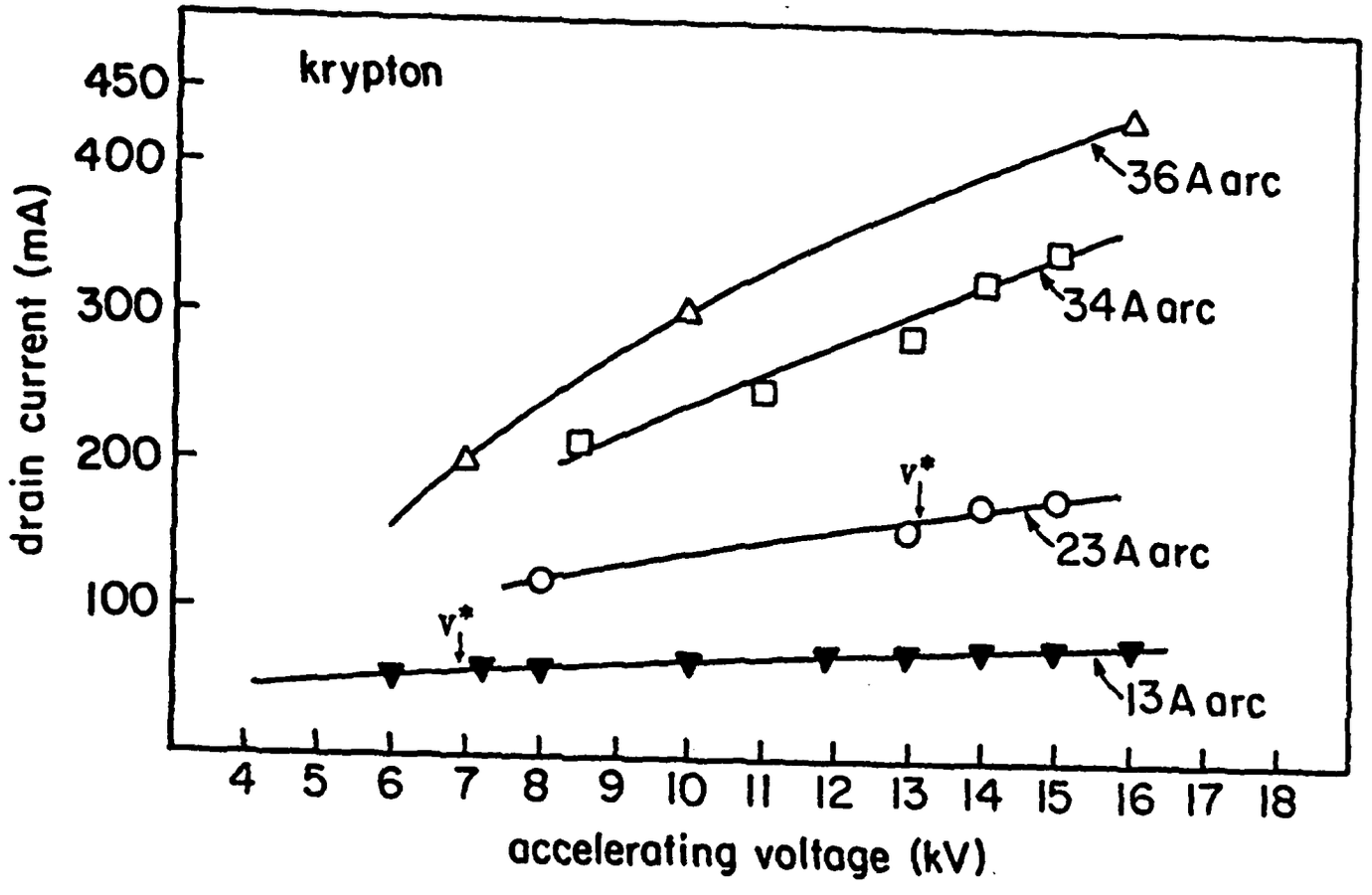

Figure 15. **Krypton beam drain current for 13 A, 23 A, 34 A, and 36 A arc discharges.**

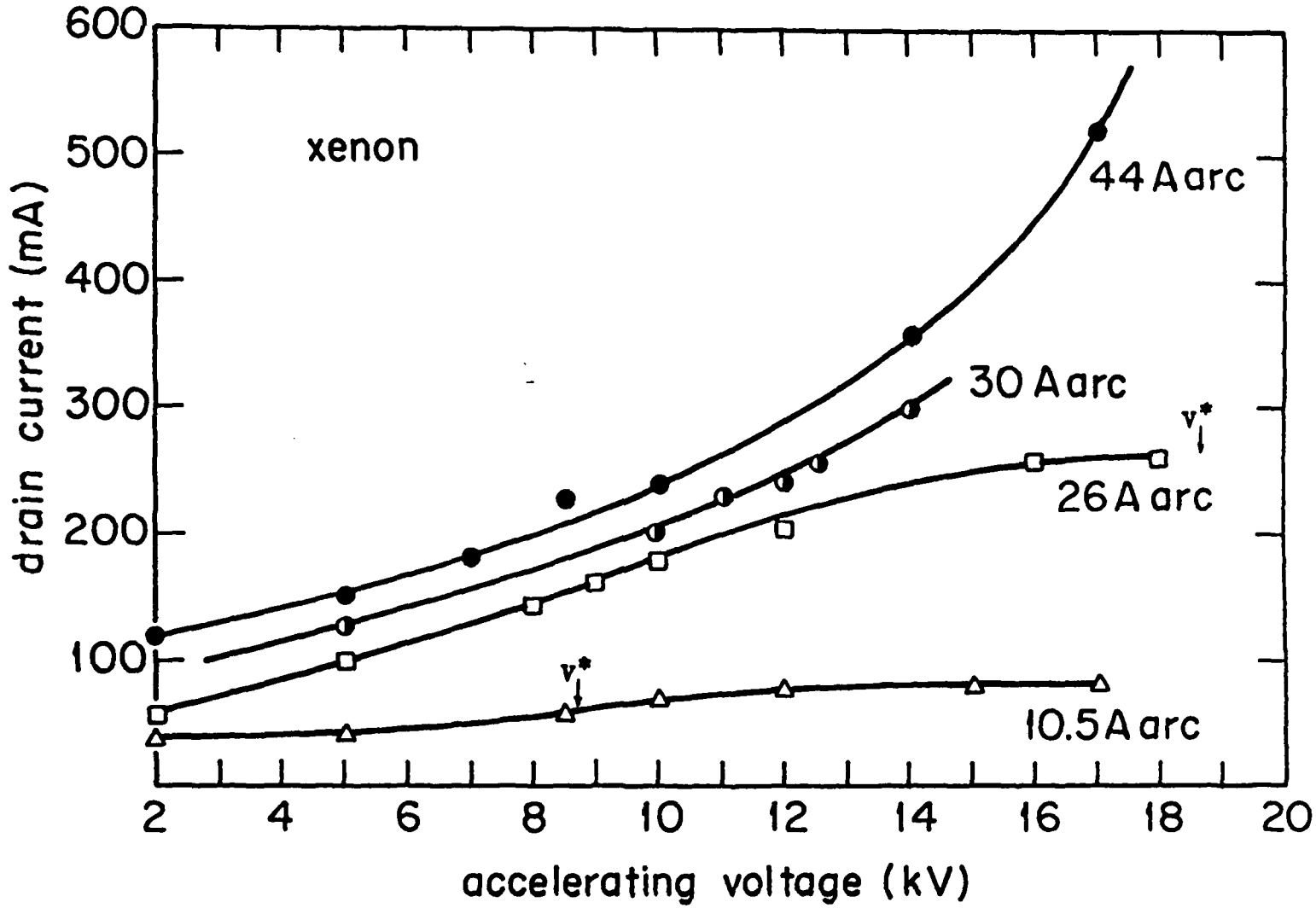

Figure 16. **Xenon beam drain current for 10.5 A, 26 A, 30 A, and 44 A arc discharges.**

the mass of the ions. Saturation ion currents agree very well with code results as seen in figures 17 and 18.

Lejeune has discussed the emissive plasma meniscus which forms in the apertures of a beam extraction grid. The data of figures 13 through 16 can be analyzed in terms of the `apparent' grid spacing caused by the emissive plasma meniscus. This analysis is summarized in Figure 19 which plots an apparent gap spacing calculated from the perveance data. Note that at the voltage V^* the apparent spacing is equal to the actual gap spacing. This means that for the optimal beam emittance an ion extraction system must be operated with a gap spacing and voltage to match V^*.

In order to focus the beam we have operated the duopigatron source with grids which incorporated both displaced aperture focusing and slight geometric focusing. The principle of displaced aperture focusing is depicted schematically in figure 20. For the parameters of our experiment the focal length for this system was approximately 4.7 meters. Two diagnostic techniques were employed to measure the neutral beam profile. One of these employed the secondary emission detector illustrated in figure 21 to obtain spatially resolved scans of beam intensity. The second detection scheme employed thermally sensitive film for which the darkness corresponded to beam intensity. A comparison of the two diagnostics in figure 22 shows excellent agreement when the peak magnitudes are calibrated.

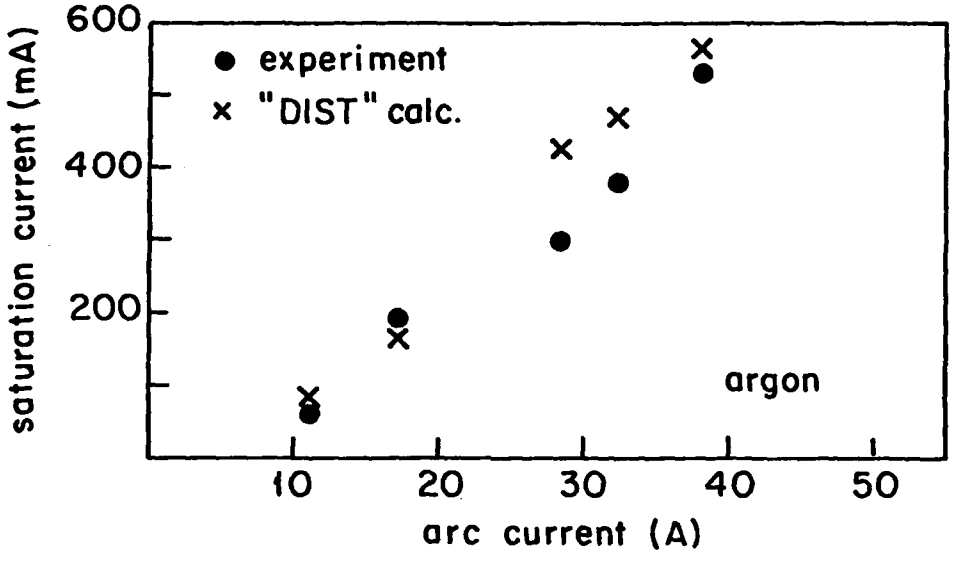
600
400
200
saturation current (mA)
experiment
"DIST" calc.
argon
10
20
30
40
50
arc current (A)

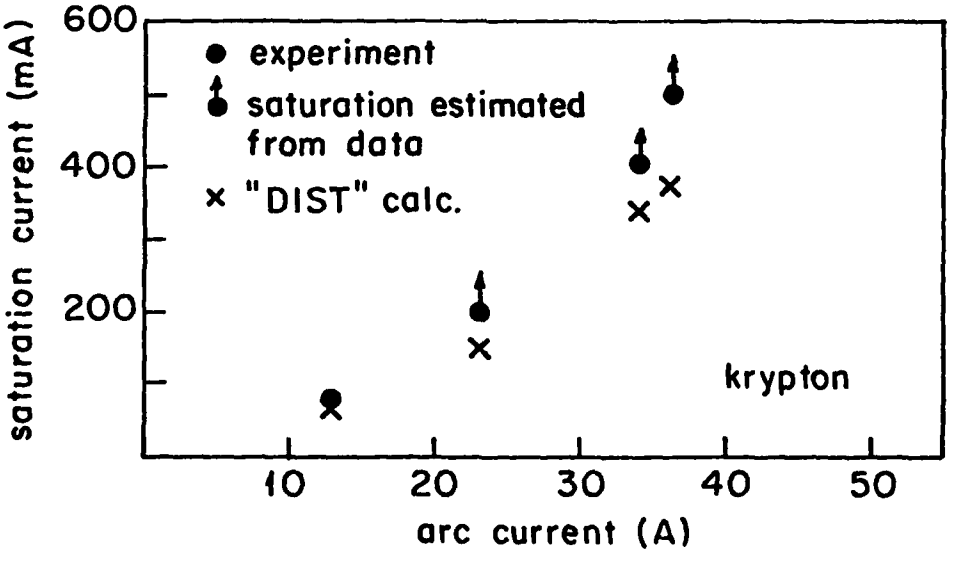
600
400
200
saturation current (mA)
experiment
saturation estimated from data
"DIST" calc.
krypton
10
20
30
40
50
arc current (A)

Figure 17.

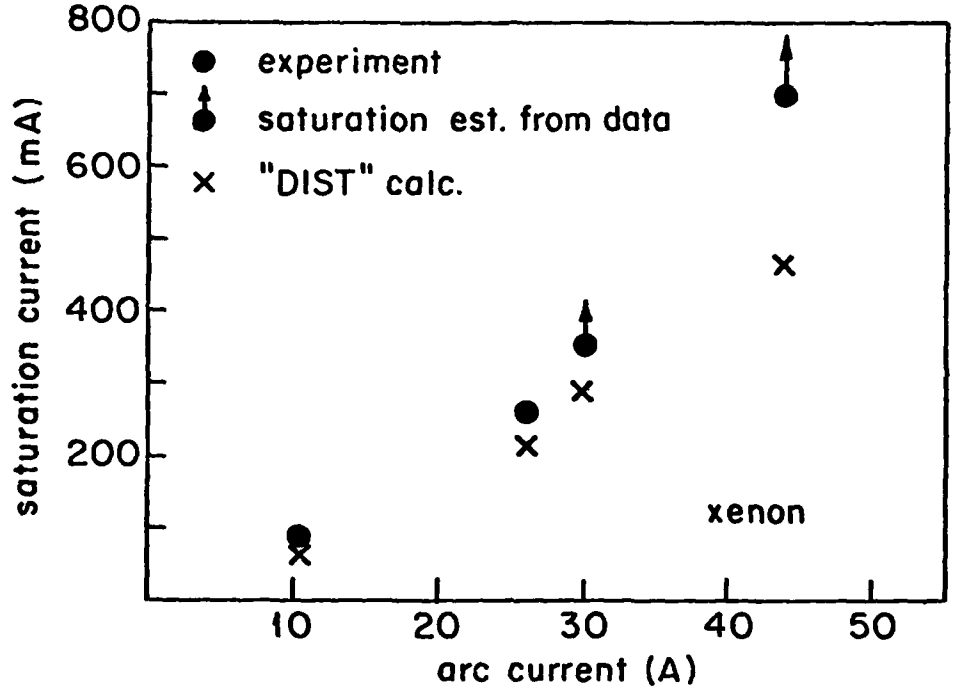
800
600
400
200
saturation current (mA)
experiment
saturation est. from data
"DIST" calc.
xenon
10
20
30
40
50
arc current (A)

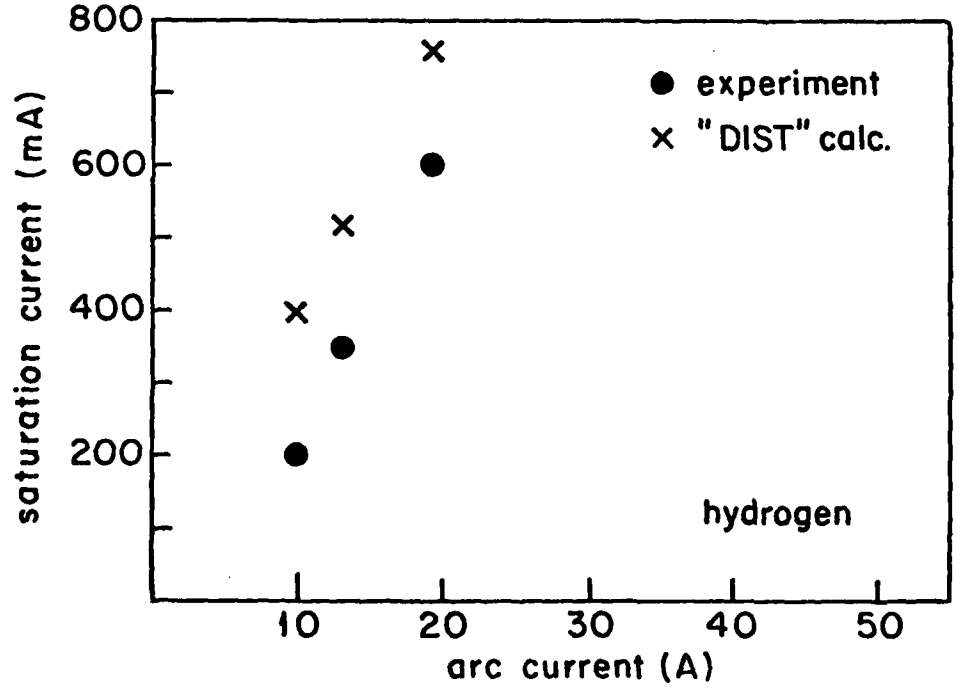
800
600
400
200
saturation current (mA)
experiment
"DIST" calc.
hydrogen
10
20
30
40
50
arc current (A)

Figure 18.

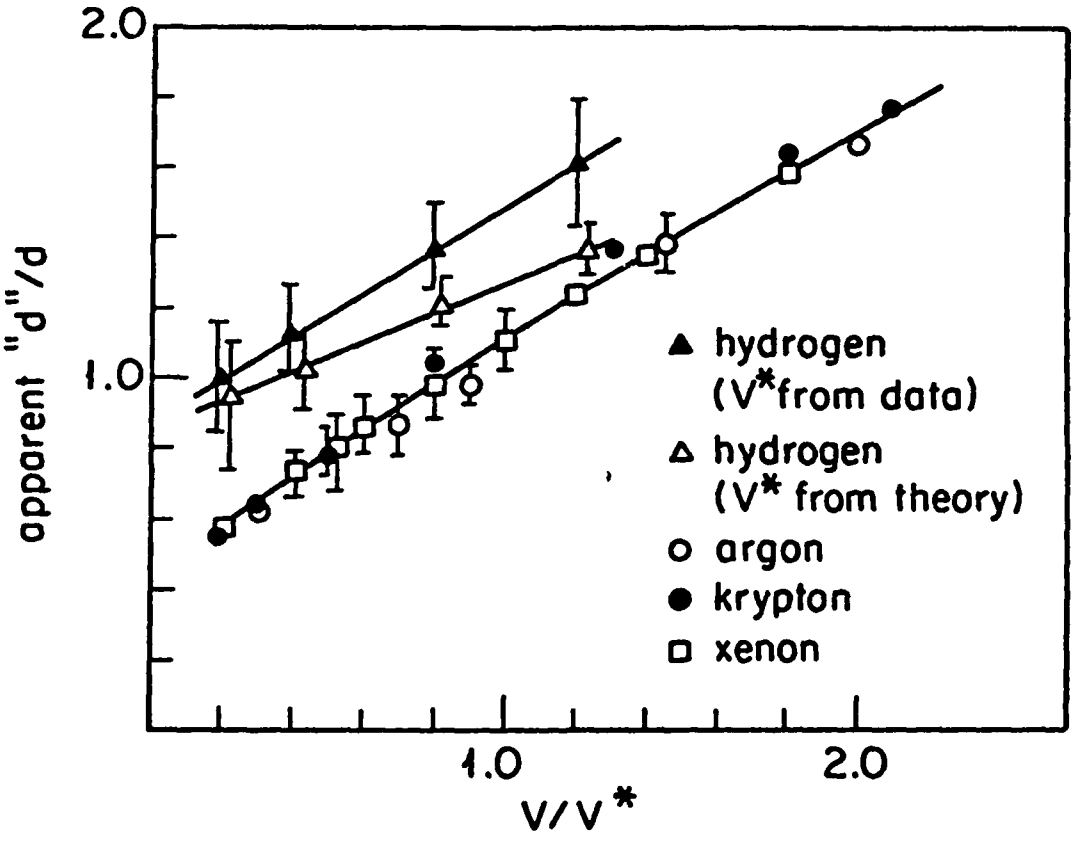

Figure 19. **Effective acceleration gap spacing calculated from perveance data.**

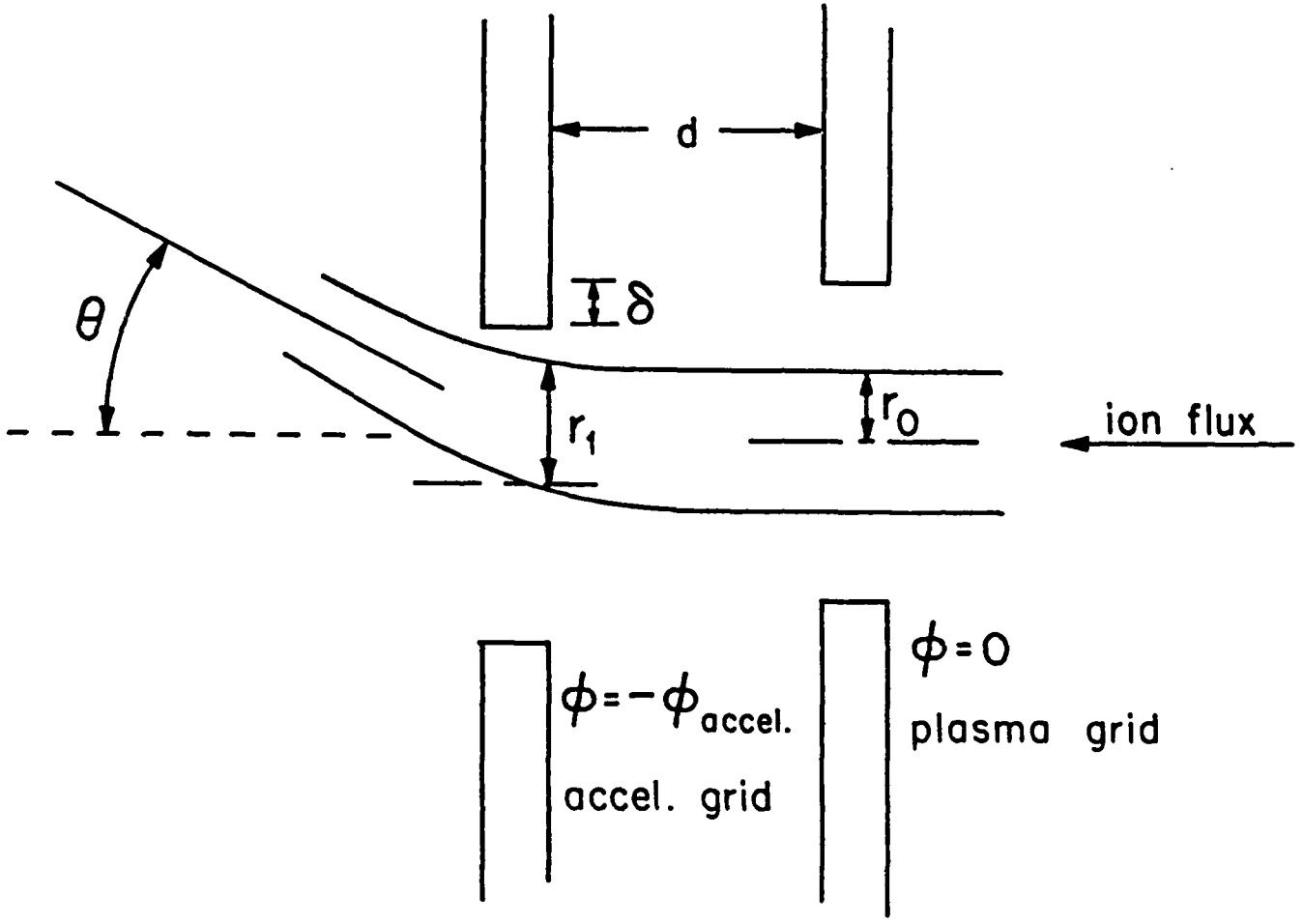

Figure 20. Beam aperture optics and displaced aperture focusing.

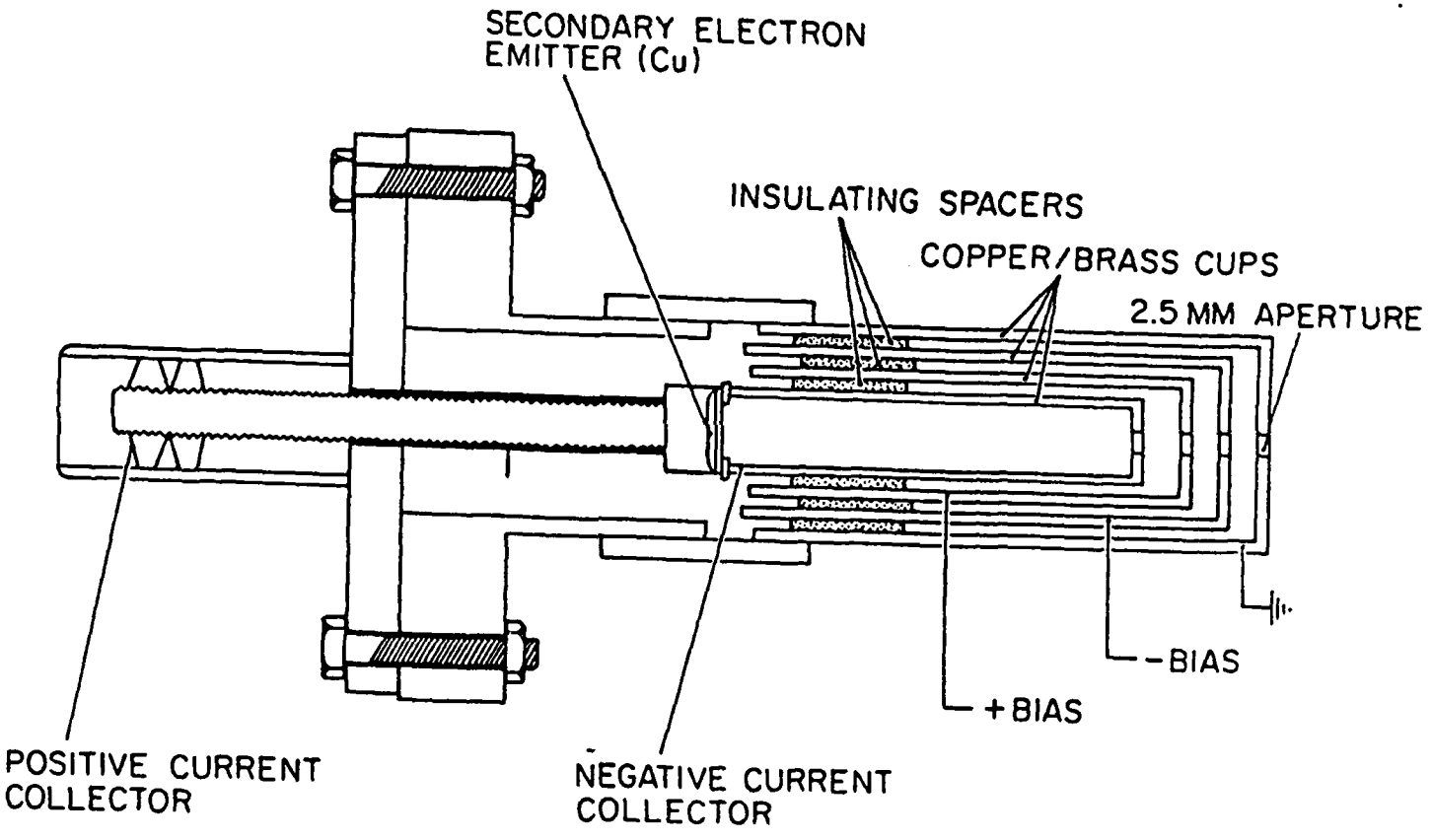

Figure 21. **Secondary emission ion and neutral particle detector.**

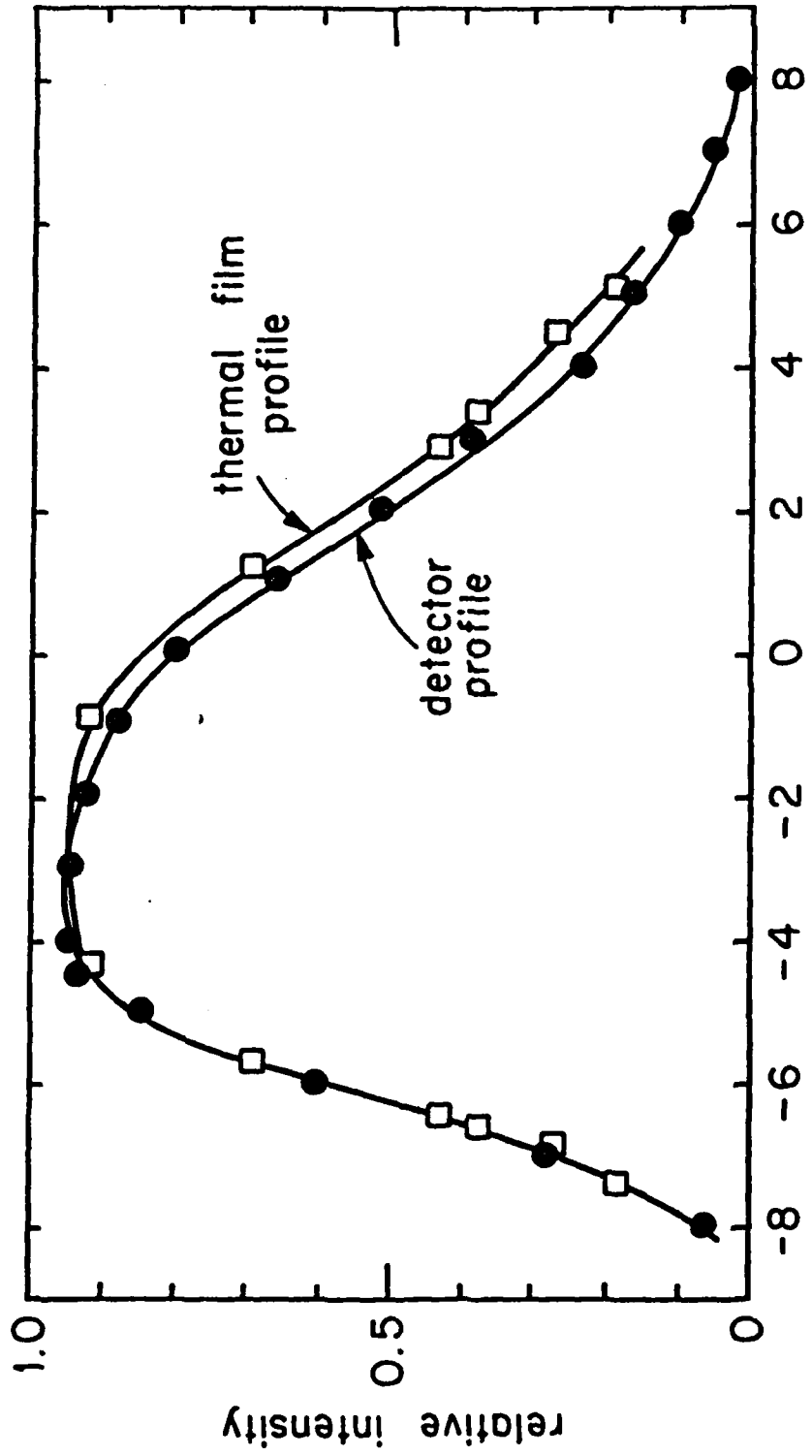

Figure 22. Comparison of argon beam profile measured by thermal film and particle detector.

Id) Laser Ablation Plasma Experiments for Particle Beam Interactions

We have developed a dedicated ruby laser facility for the generation of surface ablation plasmas. These ablation plasmas permit studies of pa .cle beam interactions with surface plasmas. Our initial experiments have aimed at characterizing the parameters of these laser ablation plasmas:

a) Density,

b) Temperature, and

c) Streaming velocity.

For this purpose we have constructed an ablation test experiment, as depicted in figure 23. A carbon target was located in a pyrex vacuum vessel. Two semicircular copper collecting plates were constructed with a small hole in the center to pass the focused ruby laser beam. The collector plates could be biased for measurements of plasma electron and ion currents. In the initial experiments the ruby laser was operated in the relaxation mode, which generates a large number of spikes for each flashlamp pulse (Figure 24). The collected ion current from a single ruby laser pulse is shown in figure 25. A preliminary scan of collector voltage versus current is given in figure 26. This probe data indicates an ablation plasma temperature between 20 and 30 eV. By spacing the two collector plates different distances from the ablation target and measuring the

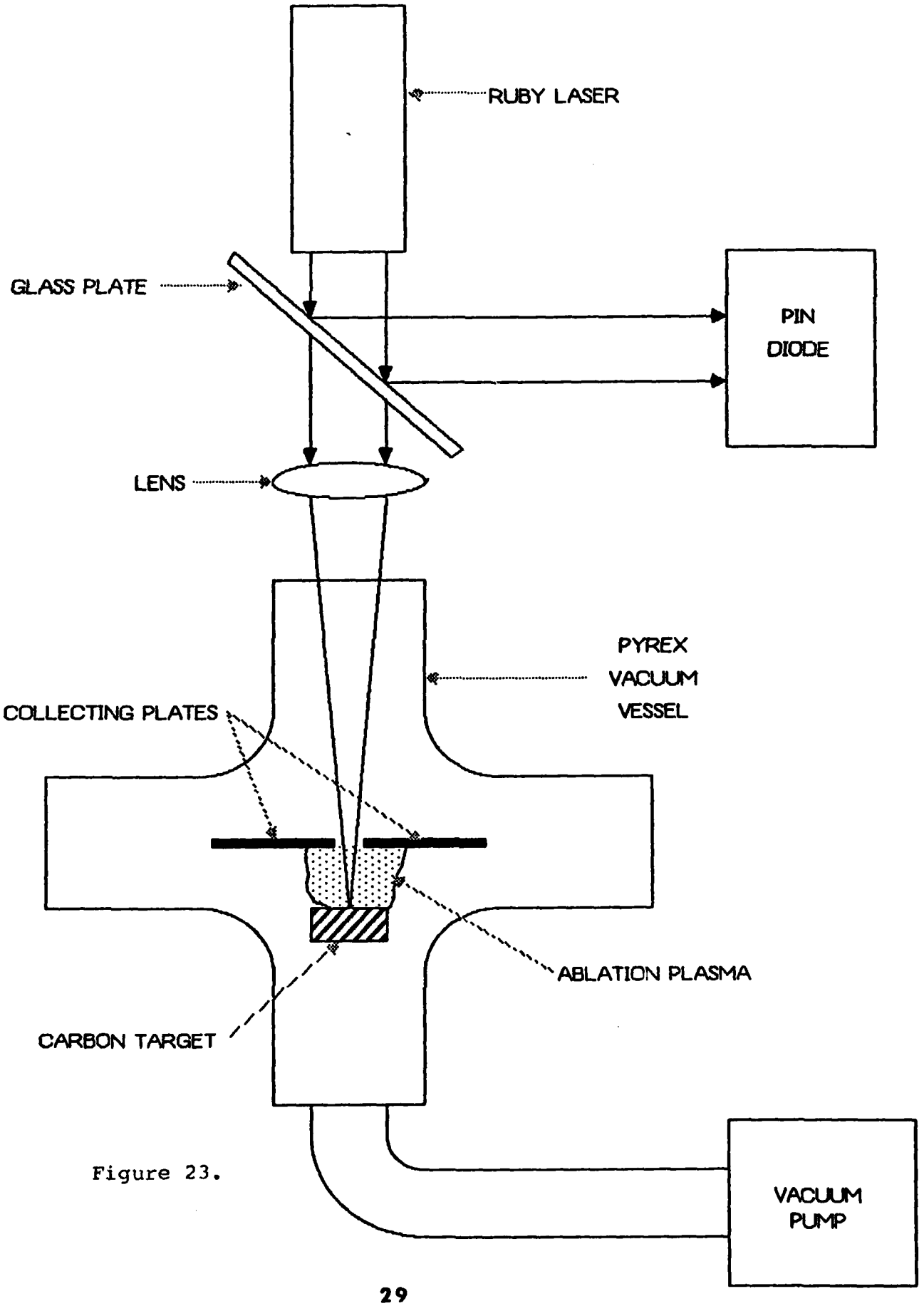
RUBY LASER
GLASS PLATE
PIN
DIODE
LENS
PYREX
VACUUM
VESSEL
COLLECTING PLATES
ABLATION PLASMA
CARBON TARGET
VACUUM
PUMP

Figure 23.

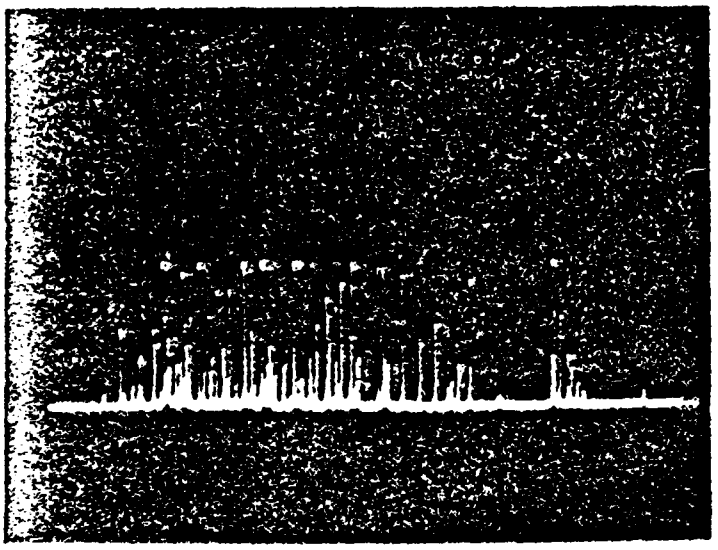

shot #194

50mV, 50μs/div

. NEUTRAL DENSITY = 4.00

Series of Laser Pulses Generated in 'Relaxation Mode'

Figure 24.

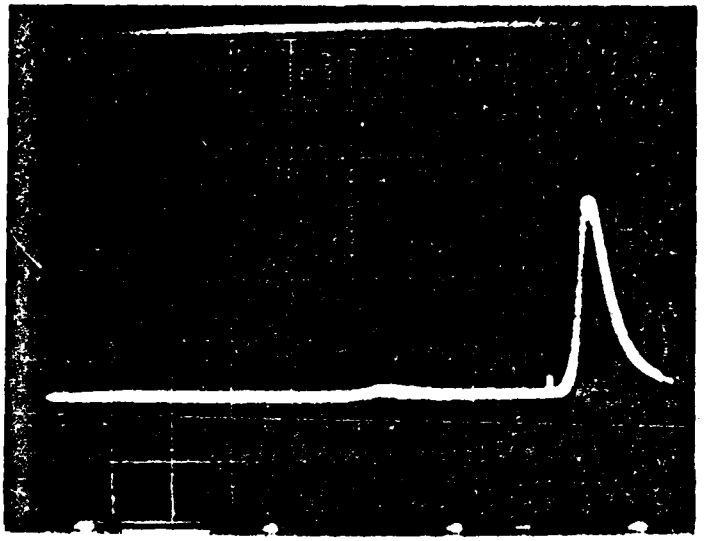

Figure 25. Collector Current @ -300V bias 0.5V/div 5us/div

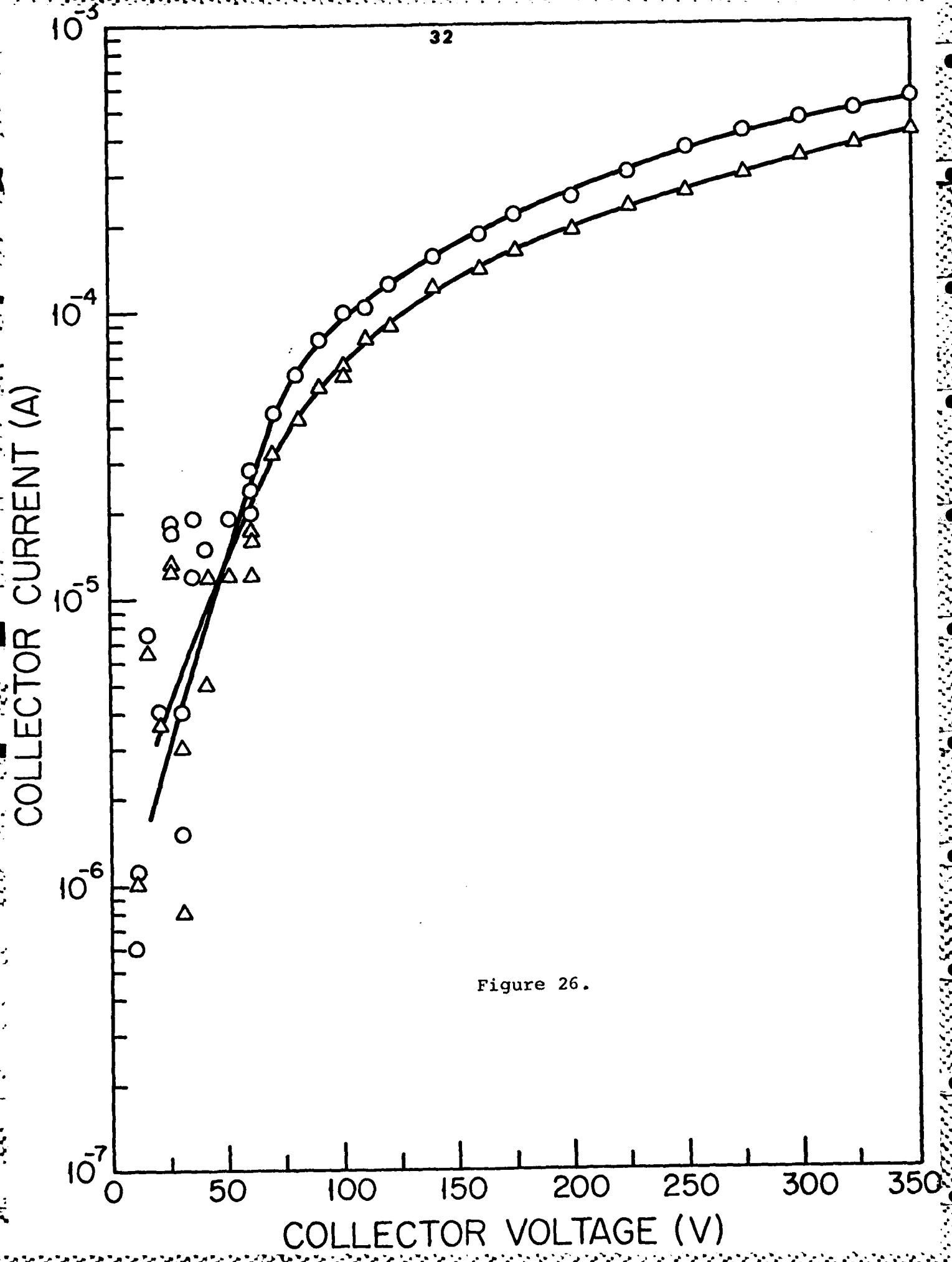
10^{-3}
10^{-4}
10^{-5}
10^{-6}
10^{-7}
COLLECTOR CURRENT (A)
0
50
100
150
200
250
300
350
COLLECTOR VOLTAGE (V)

Figure 26.

relative delay of the ion current, one can deduce the plasma streaming velocity. Our preliminary estimates place this velocity between 10^6 and 10^7 cm/sec. We are currently refining these estimates by operating the ruby laser in the Q-switched mode which gives a single, short ruby laser pulse as shown in figure 27. The beam-ablation plasma interaction configuration is depicted in figure 28. This design permits neutral or ion interactions with independently excited ablation plasmas to be studied.

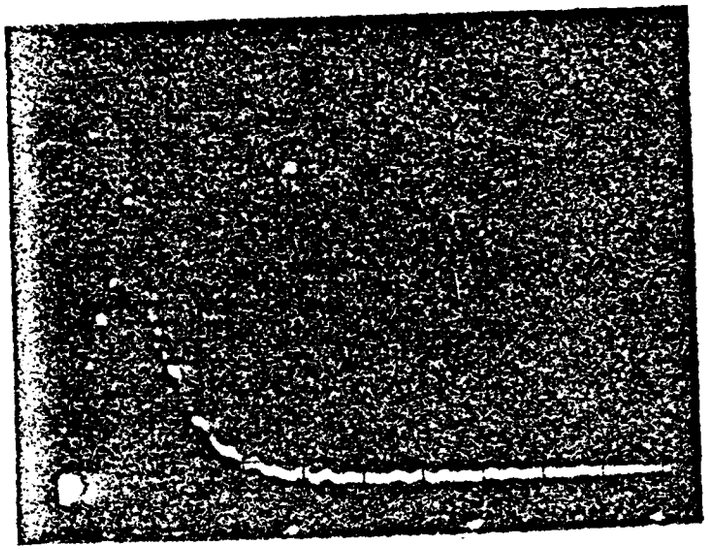

#1/2

20 mV, 0.2μs/div

ND = 12.20

Single Q-Switched Laser Pulse

Figure 27.

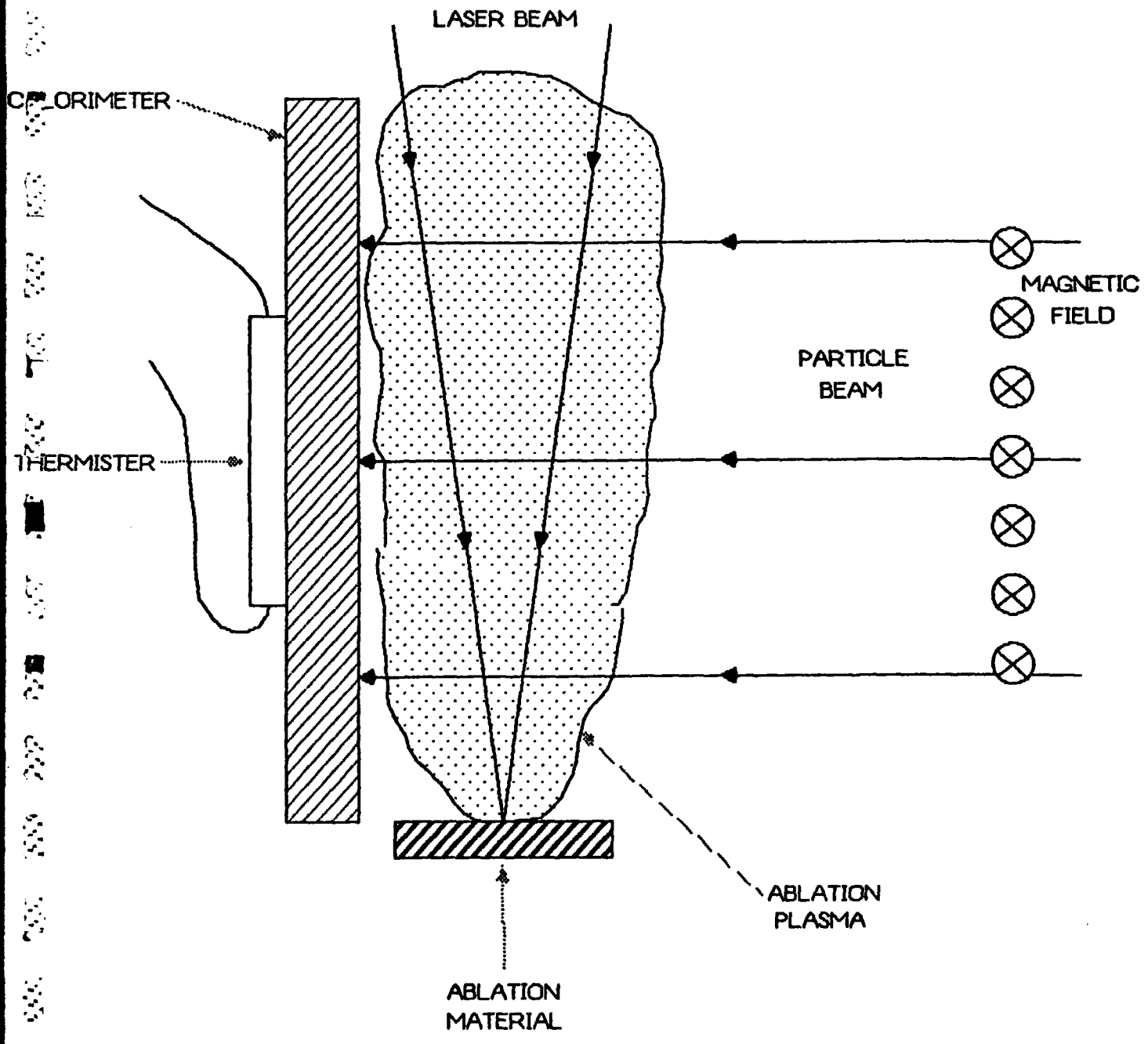
LASER BEAM
CALORIMETER
MAGNETIC
FIELD
PARTICLE
BEAM
THERMISTER
ABLATION
PLASMA
ABLATION
MATERIAL

Figure 28..

II Theoretical Program

IIa) Neutral Beam Interactions with a Solid Target

As a neutral beam interacts with a solid target, the target ionizes. This increases the number of free electrons which can then contribute to the slowing down process. Recent effort has been directed to obtain an expression appropriate for the free electron stopping power for a neutral hydrogen projectile.

Mehlhorn(1) has made a comparison of different models for ICF ablator plasmas. He favored the simple binary collision theory due to its computational simplicity. However, for our purposes the dielectric response theory(2) (also known as the polarization drag model) is most readily adapted (3,4) to a projectile with a charge distribution, in particular a neutral atom. Computational tractability may be achieved through appropriate power series expansions (5,6).

The charge density of a projectile with nuclear charge Z and N bound electrons is given by

$$\rho(\underline{r},t) = Ze\,\delta(\underline{r}-\underline{v}t) - Ne\,|u(\underline{r}-\underline{v}t)|^2$$

where e is the electronic charge and u(r) is the wave function of the bound electron. For hydrogen, Z = N = 1 and

$$u(r) = (\pi a_o)^{-3/2}\, e^{-r/a_o}$$

The Fourier transform of ρ may be written

$$\rho(\underline{K},\omega) = 2\pi\,\rho(K)\,\delta(\omega - \underline{K}\cdot\underline{v})$$

where

$$\rho(K) = e\left[Z - 16\,N a_o^{-4}/(K^2 + 4a_o^{-2})^2\right]$$

for hydrogen. Then, the polarization energy loss of the projectile is given by(3,4)

$$\frac{dE}{ds} = \frac{2e^2}{\pi v^2}\int_0^\infty \frac{dK}{K}\,|\rho(K)|^2 \int_0^{Kv} d\omega\,\omega\,\mathrm{Im}\left(\frac{-1}{\varepsilon(K,\omega)}\right)$$

where $\varepsilon(K,\omega)$ is the dielectric function.

When one is interested in high velocities, P. Sigmund and De-Ji Fu(6) have demonstrated the advantage of expanding the dielectric constant in powers of the free electron velocity at an earlier stage than is customary(5). Assuming our ablator plasma to be similar to the cold(50-200eV)(1) dense plasmas found in ICF applications, this procedure seems well suited to our problem. This permits us to use the full quantum mechanical form(2) of

the dielectric function assuming only that the plasma is isotropic. Their method rederives the result for an electron gas at rest(2) and agrees to second order in electron velocity with a later, independent result for the case of a degenerate Fermi gas at finite temperature.(7)

Following this prescription in equation 1, one obtains, after integration, the free electron contribution to the stopping power of neutral hydrogen. The results of Brandt and Kitagawa(4) (with a different dielectric function and an electronic charge density less suited to the 1-s type binding found in hydrogen) indicate that the stopping power for the neutral atoms is roughly one-half that for the bare nuclei. Preliminary calculations using our result indicate a similar trend.

For ICF applications, the dielectric response models have emphasized the collisional nature of the ablator plasmas(1). Hence, the classical collisional dielectric function (in terms of the plasma dispersion function) has been used although it is quantum mechanically inconsistent(8). However, it has been argued(9) that the effect of collisions does not qualitatively alter the shape of the dielectric function used. It is planned to compare this collisional approach (e.g. through numerical integration of equation 1) to the one outlined here to investigate the quantitative differences.

II b) Theoretical Studies of Beam Interactions with Target Ablation Plasmas

This part of the theoretical research has concentrated on the theoretical simulation of an ion/neutral beam interacting with plasma targets. The approach being taken to model this problem consists of coupling together three computational physics models. First, there is an equation of state model which is responsible for providing the following information:

1) amount of radiative cooling,

2) plasma pressure ,

3) plasma internal energy and the free electron density.

Secondly, we have employed a hydrodynamics model which predicts the temperature and density of the target as it evolves. Finally, an energy deposition model is incorporated to calculate the amount of beam energy deposited in each region of the target.

In practice, it would be virtually impossible to generalize the above models so that they could model an arbitrary target; thus far we have only considered carbon targets in our models. This will permit comparison with experiments beimg performed in our laboratory with carbon targets. Currently, we are using the CRE model, described in earlier reports, to model the equation of state information. The hydrodynamics is modelled for a one-

dimensional slab geometry with variable boundary conditions, and the energy deposition is that due to a proton beam with arbitrary current density and kinetic energies up to 10 Mev.

All three of the models have been written, tested and coupled together. The whole package should be adequate for handling plasmas with temperatures up to 1 Kev and ion densities as low as 1.0×10^{19} cm^{-3}. This density requirement is based upon a hydrodynamic scaling time of 1.0×10^{-11} sec. For larger values of this time, we can handle correspondingly lower densities.

Areas of investigation which are relevant to target radiation signatures include:

a) general x-ray conversion efficiencies,

b) effects of inner-shell radiation - such as preheat,

c) calculating the amount of K-alpha radiation that comes from the direct interaction of the proton with the target and also that due to inner-shell photoionization,

d) potential extension to general spectroscopic studies.

The study of x-ray conversion efficiencies and the general spectroscopic investigations involve direct applications of the three models. However, the other applications require that we model the transport of inner-shell radiation. To do this we have used the formalism of Duston and Davis (10) and the thresholds of Biggs and Lighthill (11). For predicting the amount of K-alpha radiation

emitted by the direct beam-target interaction, we used the experimental data of Kahn, Potter and Worley (12). Because all the inner-shell processes require knowledge of the distribution of ion stages, the calculation needs to be done at each hydrodynamic time step.

The modelling of the above applications is finished and they have been incorporated into the three major physics models. Completion has been scheduled for this summer.

References:

1.) T.A.Mehlhorn, J.Appl.Phys. 52, 6522 (1981)

2.) J.Linhard, K.Dan.Vidensk.Selsk.Mat.Fys.Medd. 28,(8) (1954)

3.) T.L.Ferrell and R.H.Ritchie, Phys.Rev.B 16, 115 (1977)

4.) W.Brandt and M.Kitagawa, Phys.Rev.B 25, 5631 (1982)

5.) J.Linhard and A.Winther, K.Dan.Vidensk.Selsk.Mat. Fys.Medd. 34,(4) (1964)

6.) P.Sigmund and De-Ji Fu, Phys.Rev.A 25, 1450 (1982)

7.) G.Maynard and C.Deutsch, Phys.Rev.A, 26, 665 (1982)

8.) E.Nardi,E.Peleg, and Z.Zinamon, Phys.Fluids, 21, 574 (1978)

9.) G.Bekefi, in Plasma Physics, edited by C.DeWitt and J.Peyraud (Gordon and Breach,New York 1972),p.1

10.) D. Duston, R. W. Clark, J. Davis, and J. P. Apruzese, Phys. Rev. A 27, 1441 (1983)

11.) F. Biggs and R. Lighthill, Sandia Laboratories Report No. SC-RR-71 0507, Reprinted May 1982

12.) J. M. Kahn, D. L. Potter, and R. D. Worley, Phys. Rev. 139, 6A, 1735 (1965)

Appendix I

U. S. Citizen Graduate Students Engaged in This Research

---

1) P. D. Weber, Ph. D., Dissertation defended March 19, 1984, (Supported on Fellowship)

2) R Kensik, Ph. D. Candidate, (Supported by AFOSR)

3) W. Thornhill, Ph. D. Candidate, (Supported by AFOSR)

4) J. Meachum, Ph. D. Candidate, (Supported by AFOSR)

5) M. Cuneo, Ph. D. Candidate (Supported by Fellowship)

6) E. Pitcher, M.S. Candidate (Partial AFOSR support)

Appendix II

Research Publications and Conference Papers Relating to This Contract

---

1) "Intermediate and High Mass Ion Beams from a 10 cm Duopigatron ion Source", P. D. Weber and R. M. Gilgenbach, Plasma Chemistry and Plasma Processing, Vol. 4, page 75, (1984)

2) "Neutral Hydrogen Stopping Power in Matter", R. Kensik, R. S. B. Ong, and J. J. Duderstadt, Bull. Am. Phys. Soc., Vol. 28, page 1201, (1983)

3) "Mass Dependence of Ion Extraction from Duopigatron Source Plasmas", P. D. Weber, R. M. Gilgenbach, and M. L. Brake, Bull. Am. Phys. Soc., Vol. 28, page 1201, (1983)

4) "Neutral Beam - Low Z Target Interaction", W. Thornhill, J. J. Duderstadt, and R. S. B. Ong, Bull. Am. Phys. Soc. Vol. 28, page 1256 (1983)

Plasma Chemistry and Plasma Processing, Vol. 4, No. 2, 1984

Intermediate and High-Mass Ion Beams from a 10-cm Duopigatron

P. D. Weber[1] and R. M. Gilgenbach[1]

Received December 7, 1983; revised February 22, 1984

Experimental studies of a 10-cm Duopigatron as a source of argon, krypton, and xenon ion beams are reported. Source plasma instabilities are examined, and the mass dependence of oscillation frequencies and instability onset conditions are determined. Arc current and density oscillations are found to be associated with ion acoustic fluctuations with frequencies scaling as $1/M^{1/2}$. Langmuir probe measurements within the source plasma double layer are used to indicate the physical mechanism responsible for the observed large-amplitude arc current shifts. Ion beams have been extracted at energies up to 18 kV, and drain currents up to 540 mA for argon, 440 mA for krypton, and 520 mA for xenon have been achieved with source plasma densities in the range 10^{11}–10^{12} cm^{-3}. Excellent agreement with existing theoretical models has been obtained in the mass and density dependence of the extraction current, as well as the voltage at which transition from space-charge limited to ion saturation emission occurs.

KEY WORDS: Duopigatron; ion source; instability; source plasma; ion acoustic; sheath model; noble gas.

1. INTRODUCTION

In recent years a great deal of research has concerned the generation of dense ion source plasmas for high-current beam extraction. The duopigatron is an important ion source which has been extensively developed for neutral beam heating systems in plasma fusion experiments. A series of increasingly larger and more powerful duopigatron sources has been developed in the U.S. (at Oak Ridge National Laboratory[1–3] and in Japan,[4] to provide hydrogen and deuterium beams of up to tens of amperes at energies greater than 100 keV. Such sources have been used for heating many of the large magnetic confinement plasma devices.

[1] Department of Nuclear Engineering, The University of Michigan, Ann Arbor, Michigan 48109.

0272-4324/84/0600-0075$03.50/0

In parallel with the development of these high-power sources, work has been performed in France[5-7] and the Federal Republic of Germany[8] to develop and study the duoplasmatron and small-area duopigatron as sources of both hydrogen and noble gas ions. Beam currents of tens of milliamperes at up to 30 kV have been reported for duoplasmatron designs and a multiple-discharge duopigatron design.

The purpose of the experimental study reported here is to examine the performance of a large-area (ORNL type) duopigatron as a source of intermediate and high-mass ion beams including argon ($A = 40$), krypton ($A = 84$), and xenon ($A = 131$). There exist a number of important processing applications for large-current, high-mass beams including dry etching of semiconductors[9] and surface modification of materials.[10] Other potential uses for such beams include plasma diagnostics, heavy-ion plasma heating, and preinjection into high-energy ion accelerators such as the RF quadrupole.

2. EXPERIMENTAL CONFIGURATION

The ion source used in the present study is a 10-cm duopigatron of the type developed at Oak Ridge National Laboratory. Figure 1a depicts this duopigatron as configured for the present study. The discharge is initiated by thermionic emission from an oxide-coated, tungsten-wound, tantalum cathode. Feed gas enters the cathode region near the base of the filament. The formation of a double layer of electrons and ions between the cathode plasma and the anode (Fig. 1b) accelerates electrons into the anode volume, following the field lines of the source magnet. These primary electrons, with energies of 30–90 eV, ionize the gas in the anode region to form the source plasma. The first extraction grid is maintained at a negative potential with respect to the source plasma, by means of a 350-Ω load resistor between the grid and second anode. The resulting potential profile reflects primary electrons, thus establishing a reflex (*P*enning *I*on *G*auge type) discharge between the double layer and the grid. This increases the path length and ionization efficiency of the primary electrons. Ions escape from the source plasma either by crossing the double layer toward the cathode plasma (necessary to maintain stability of the double layer) or by crossing the first grid sheath boundary to be accelerated by the extraction grids.

A triode extraction grid arrangement was used, with the second grid biased negatively at 10% of the primary accelerating voltage. The grids were approximately 52% transparent with 369 aperatures of 3.75 mm diameter in a 10-cm-diameter hole pattern.

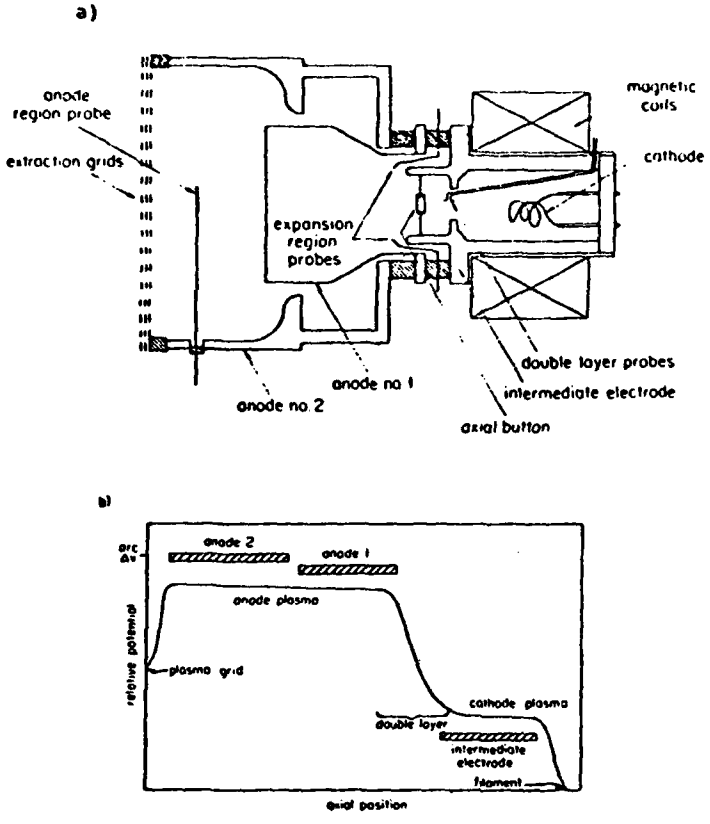

Fig. 1. (a) 10-cm diameter Duopigatron ion source, showing location of plasma probes; (b) potential profile through Duopigatron, showing double layer, and plasma grid sheath (see Ref. 3).

The entire experiment is shown schematically in Fig. 2. Downstream of the ion source is a 38-cm-long, 30-cm-diameter neutralization tank in which a neutral gas background density is maintained by excess feed gas from the source. A gate valve, 15-cm-diameter drift tube, and target tank complete the beamline. Overall length from the extraction grids to the end of the target tank is approximately 163 cm.

The high-voltage beam extraction circuit utilized an ignitron switched and crowbarred capacitive discharge system. A current-limiting resistor of 80 Ω was used in series with the source, while a parellel resistor to ground was used to stabilize the current through the firing ignitron.

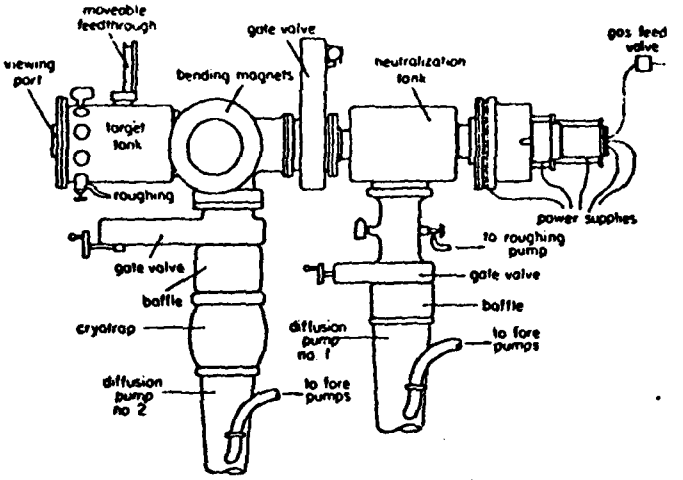

21033 **Fig. 2. Ion source and beamline experimental configuration.**

3. SOURCE PLASMA EXPERIMENTS

For argon, krypton, and xenon, reproducible source plasma discharges were obtained with total arc currents up to approximately 40 A (limited by power supplies). In this study, arc current was controlled primarily by adjusting gas feed, rather than applied arc voltage. Lower gas feed rates and anode-region pressures were needed to sustain arcs in krypton and xenon than in argon. At an arc voltage of 100 V and a source magnet current of 7.1 A (corresponding to a peak magnetic field of 115 G), arc currents of approximately 22 A were obtained for argon at a gas feed rate of 0.14 Torr-liter/sec and a pressure of 3 mTorr, for krypton at 0.1 Torr-liter/sec and 1 mTorr, and for xenon at 0.05 Torr-liter/sec and 0.5 mTorr. This trend toward lower required pressures for the higher-mass gases can be explained to a large extent by observing that the ionization cross sections for 30-eV electrons are approximately $2\pi a_0^2$, $3\pi a_0^2$, and $4.3\pi a_0^2$ for argon, krypton, and xenon, respectively[11] (where a_0 is the first Bohr radius).

A source plasma instability has been observed for argon, krypton and xenon which is more pronounced than that observed for hydrogen under similar conditions. Because of the sensitivity of this instability to gas feed rate and its dual-mode character, it is believed to be an arc starvation instability of the type previously observed in studies of duoplasmatron source by Lejeune[12] and by Winter and Wolf.[13] The instability is evidence by a rapid shift between a "normal" (high-current) mode, and an "arc starvation" (low-current) mode. The arc-starvation mode is characterized

by a low neutral gas density, with a resulting ionization density insufficient to provide the required ion flux to maintain a stable intermediate electrode double layer in accordance with the Langmuir[14] sheath criterion $j_e/j_i = \gamma(M_i/m_e)^{1/2}$, where γ is a constant or order unity. In the experiments reported here, the parametric behavior of this instability has been studied.

To monitor the effects of this instability on the double-layer potential profile, a double probe was devised to measure within the double layer. The two probes, spaced 6 mm apart axially, did not necessarily bound the entire double layer, but did provide a relative measurement of the slope of the potential profile in this region.

Figures 3a and 4a show the current (lower traces) and double-layer potential difference (upper traces) for low-current-mode operation in argon and krypton, respectively. At a discharge current of approximately 1 A, probe potential differences of 20 and 35 V are measured. Figures 3b and 4b show the high-current mode (during which current was ramped from approximately 3–12 A during 500–600 msec pulses). In this case, the probe potential difference is only 10 V. Further, the overall arc voltage drops with increasing current. Thus, the high-current mode is characterized by a flatter and lower double-layer potential profile, and correspondingly lower primary-electron energy.

Figures 3c and 4c show the argon and krypton discharges during mode shifts between the low- and high-current cases. This mode shift can be explained by examining the behavior of the ionization cross sections in the range 30–100 eV. The cross sections peak at about 100 eV and begin to drop rapidly below about 40 eV.[11] For the low-current discharge most of the arc voltage drop of 100–110 V occurs across the double layer, producing high-energy primary electrons with high ionization efficiency. The ions thus produced diffuse to the double layer to contribute to an increased ion flux toward the cathode. This permits (according to the sheath criterion) an increased electron flux and higher arc current. Now, however, the lowered double-layer accelerating potential produces lower-energy primary electrons with decreased ionization efficiency. A drop in ion production reduces the double-layer ion flux, forcing a drop in arc current. When the gas density is sufficient to sustain an adequate ion generation rate, with the lower-energy primary electrons, the mode shifting ceases and the arc enters a relatively stable high-current mode.

In this mode, however, the arc current displays a lower-amplitude sinusoidal oscillation as plotted in Fig. 5. It should be noted that these observed fluctuation frequencies (at 6 A magnet current) follow an ion acoustic mass scaling to within better than 10%. Ion density fluctuations occur with negligible delay throughout the anode plasma volume, suggesting that these are transmitted by streaming electrons. It should also be noted

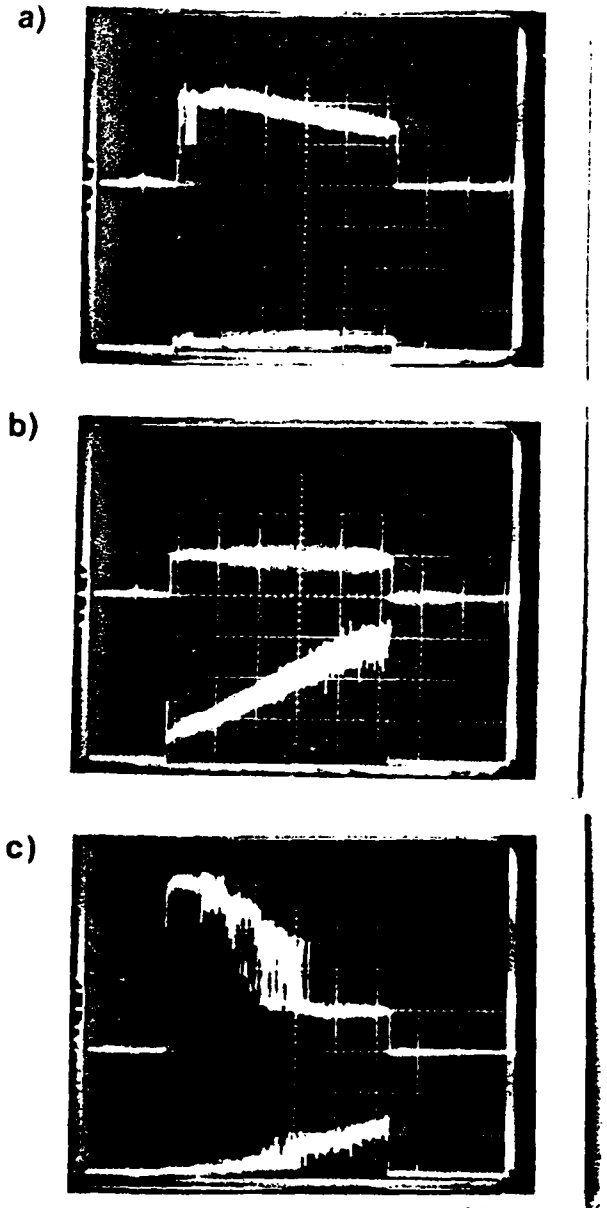

Fig. 3. Double-layer floating potential difference (upper trace, 10 V/div) and arc current (lower trace, 4 A/div) for argon in (a) low current mode, (b) high current mode, and (c) mode-shifting condition. Time scale is 100 msec/div.

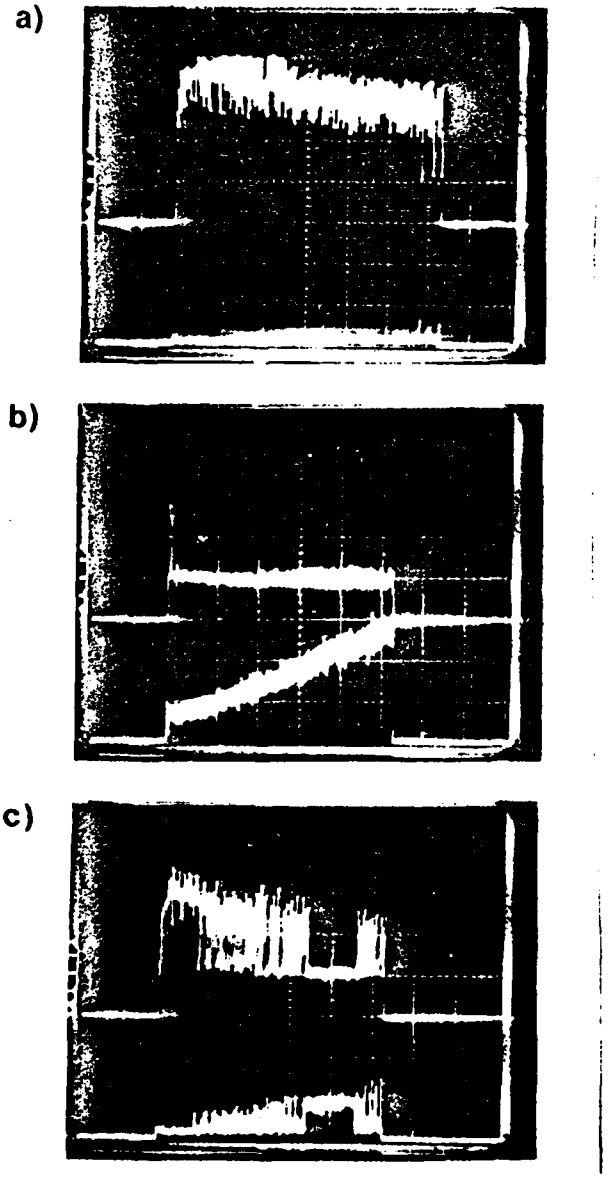

Fig. 4. Double-layer floating potential difference (upper trace, 10 V/div) and arc current (lower trace; 4 A/div) for krypton in (a) low current mode, (b) high current mode, and (c) mode-shifting condition. Time scale is 100 msec/div.

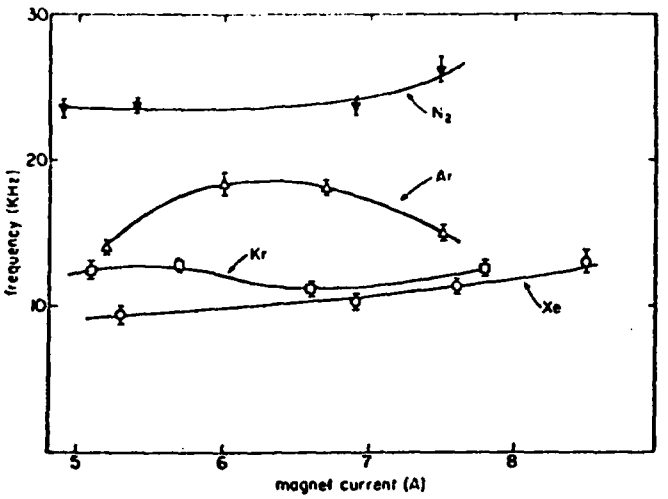

21041 **Fig. 5.** Arc oscillation frequency as a function of source magnet current.

that the insensitivity of the oscillation frequency to magnetic field rules out any EXB rotational oscillation as the cause.

Unlike the duoplasmatron used in the studies cited above,[12,13] the duopigatron is characterized by a reflexing electron discharge in the anode region. To determine the effect of these electrons on the mode shift instability, discharges were run with and without the load resistor between the plasma grid and the anodes. Without the resistor (grid shorted to anodes) the reflexing electrons will be suppressed. In this case, the discharge remains in the low-current mode for a longer period, and becomes destabilized in the high-current mode. Two possible mechanisms may be responsible for this behavior. The reflexing electrons normally help to neutralize the space charge on the anode side of the double layer. Without these electrons the potential profile could be steepened, and the double layer would resist the transition to the smoother potential profile characteristic of the high-current mode. Also, the reflexing electrons contribute to the ionization density, and their absence would have the same effect as a lowered gas density. Probe measurements of the anode-region ion density and the potential slope in the double-layer region indicated a slight decrease in ion density without the reflexing electrons, but no measurable change in the double layer near the snout. The reflexing electrons apparently influence the mode shift instability through their effect on ionization density, rather than space charge.

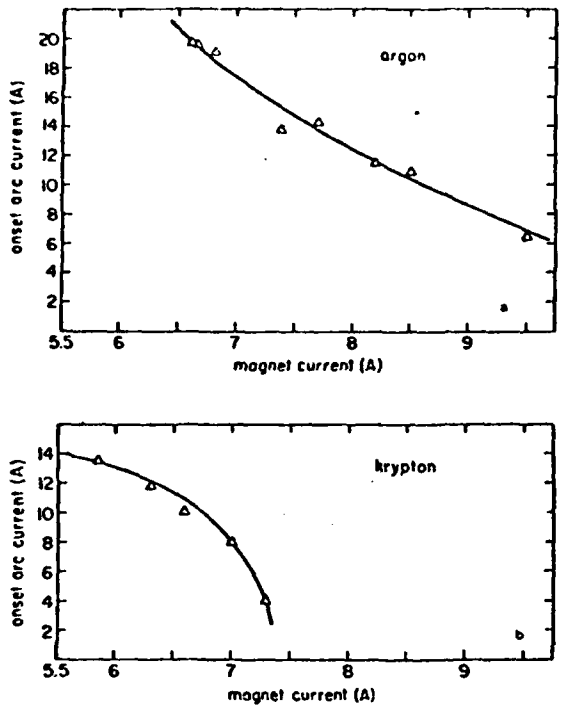

Fig. 6. Mode shift onset current as a function of source magnet current for (a) argon and (b) krypton.

Figures 6a and b show the mode-shift onset current as a function of source magnet current for argon and krypton. At higher field strengths a lower total arc current is required to initiate the instability. Studies by Jacobsen and Eubank[15] have shown that the double-layer potential difference is proportional to the temperature of the double-layer electrons. Electron loss will be controlled by Bohm diffusion where $D_{\perp \text{Bohm}} \propto T/B$. Thus for a given steady-state density condition, with constant electron generation and loss, the double-layer electron temperature (and potential difference) will be proportional to the magnetic field strength. As the field strength is increased, the double-layer voltage difference increases. Thus (for a fixed power-supply voltage), the maximum current attainable, before forcing a change in the double-layer configuration to the high-current mode, will decrease. The difference in instability onset current between argon and krypton is believed to be due to a difference in arc power-supply voltage.

4. BEAM EXTRACTION

4.1. Review of Extraction Theory

The ion current which can be extracted from a source plasma is limited by the density and mobility of the source ions. The theory developed by Lejeune[16] to predict saturation ion extraction currents utilizes a sheath boundary model to determine the potential profile and ion density near a biased electrode. The region between the bulk source plasma and the electrode (in this case an extraction grid) is considered to consist of two regions; a presheath region in which $n_e = n_i$, but $E \neq 0$, and the sheath region in which $n_e < n_i$ and $E \neq 0$. The axial energy of ions crossing from the presheath to the sheath regions is found to be[17]

$$W_i = \tfrac{1}{2}kT_e \tag{1}$$

By assuming the ion energy in the bulk plasma region to be small relative to the electron energy, the potential difference across the presheath is found to be

$$V_{ps} = kT_e/2e \tag{2}$$

Thus the electron (and ion) density at the sheath–presheath boundary is

$$n_{es} = n_{is} = n_{e0} \exp(-eV_{ps}/kT_e) \tag{3}$$

Substituting for V_{ps} we find

$$n_{is} = 0.61\, n_{e0} \tag{4}$$

The ion saturation current then becomes[16]

$$j_i = 0.61\, n_{e0}\, e \quad (kT_e/M_i)^{1/2} \tag{5}$$

This derivation assumed a Maxwellian distribution of electron velocities in the presheath region. However, the duopigatron is characterized by a large number of primary electrons reflexing between the plasma grid and the double layer at the intermediate electrode. These electrons, which determine the potential of the plasma grid, will enter the presheath region with energies of approximately 30–90 eV (compared to a bulk electron temperature of 1–2 eV). To more accurately characterize the sheath and the resulting ion saturation current, modifications to the Bohm theory have been proposed by Prewett and Allen[18] and Uehara *et al.*[19] These theories include the effects of a second, higher-energy, group of electrons in the Poisson equation. According to Prewett and Allen, the boundary between the sheath and presheath is characterized by a potential V_0, where

$$eV_0/kT_e = \frac{\tfrac{1}{2}(n_{i0}/n_{e0})}{(1 - j_h/j_e)} \tag{6}$$

where j_b is the current density of beam electrons and

$$j_c = n_{e0}\, e \quad (kT_e/m_e)^{1/2}(2eV_0/kT_e)^{3/2} \tag{7}$$

Note that for $n_{e0} = n_{i0}$ and $j_b = 0$ this model reduces to the Bohm prediction.

Typical parameters of this experiment have been measured by Langmuir probe:

$$j_b = 0.5 \text{ A/cm}^2$$

$$kT_e = 2 \text{ eV}$$

$$n_{e0} = n_{i0} = 1 \times 10^{11} \text{ cm}^{-3}$$

Solving Eqs. (6) and (7) iteratively we find

$$V_0 = 0.72kT_e/e \tag{8}$$

Then we obtain the ion density from

$$n_i = n_{e0} \exp(-eV_0/kT_e) = 0.49n_{e0} \tag{9}$$

and the ion velocity becomes

$$\tfrac{1}{2}M_i v_i^2 = eV_0 \tag{10}$$

Substituting for V_0 from Eq. (8) we have

$$v_i = (1.44kT_e/M_i)^{1/2} \tag{11}$$

The ion current can then be written

$$j_i = 0.58n_{e0}\, e \quad (kT_e/M_i)^{1/2} \tag{12}$$

Thus, for the parameters of this experiment, the ion saturation current reaching the plasma grid should not vary significantly from the Bohm criterion prediction of Eq. (5).

4.2 Beam Extraction Experiments

Argon, krypton, and xenon ion beams have been generated, varying extraction voltages and source plasma densities to determine the scaling of extracted current with these parameters (Figs. 7a, b, and c). For argon, the high-voltage drain current appears to approach a plateau for each arc current value, as predicted by the Lejeune theory. However, for krypton and particularly xenon, drain current does not saturate for the high arc current cases. The argon drain current scales approximately as $I_{arc}^{5/4}$. Since ion density scales approximately as the arc current, and electron temperature increases slightly with higher current, this scaling is reasonable and in good agreement with extraction theories [Eq. (5)]. It appears, however, that for the higher-

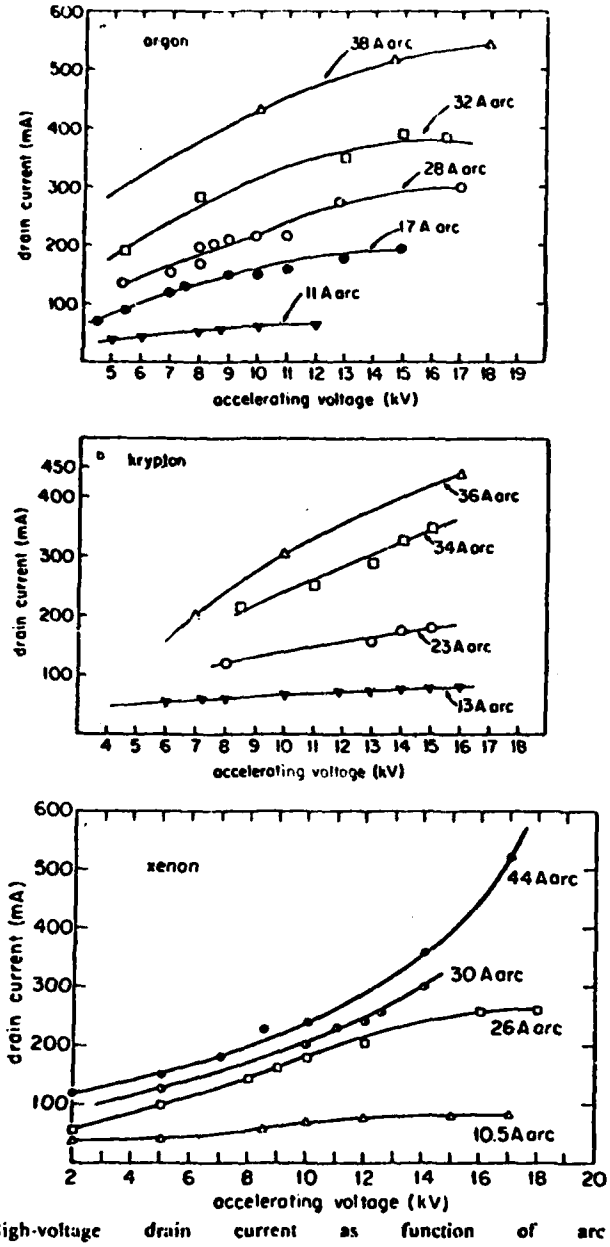

Fig. 7. High-voltage drain current as function of arc current and accelerating voltage for (a) argon, (b) krypton, and (c) xenon.

mass ions a somewhat different dependence is involved. Lejeune[16] provides a prediction of the accelerating voltage at which the extracted current should undergo the transition from space-charge limited emission to the ion saturation regime:

$$V^* = [9j_+ d^2/4\varepsilon_0(2e)^{1/2}]^{2/3} M^{1/3} \tag{13}$$

where j_+ is the ion current density of Eq. (5) and d is the grid spacing (14 mm). This equation gives the voltage at which the space-charge limited (Child–Langmuir) current equals the ion saturation current of Eq. (12). Applying this prediction to the experimental case, for a drain current of 400 mA, V^* is 18 kV for argon, 23 kV for krypton, and 27 kV for xenon. At 160 mA drain current, V^* is 11 kV for argon, 14 kV for krypton, and 15 kV for xenon (see Figs. 7a, b, and c). Thus, for argon we operated in the region of $V \geq V^*$; for krypton, in general, $V \geq V^*$; and for xenon $V < V^*$.

For xenon, at the higher arc currents, the extraction current is apparently not limited by ion density and mobility, as the sheath extraction theory assumes, but rather by normal space-charge limited emission. The xenon extraction currents, for the dense-source plasmas, in the range 10–17 kV, follow a $I \propto V^{3/2}$ dependence as predicted by the Child–Langmuir law for space-charge limited emission at $V \ll V^*$. In this regime, the ion density is well above that required to provide the measured extraction current, and thus the source plasma is acting as an emissive surface with an excess supply of ions.

At the other extreme, the argon extraction closely follows the Lejeune sheath model extraction theory, both in terms of extraction current scaling with ion density, and in its approach to saturation with increasing acceleration voltage. Between these extremes, the krypton-extracted currents follow an almost linear dependence indicating a transition from space-charge limited current to a saturable current as V approaches V^*.

For the argon extraction currents, which appear to follow the sheath extraction theory, excellent quantitative agreement exists between theory and experiment. For example, at an arc current of 32 A, Langmuir probe measurements indicate a peak plasma density of 6×10^{11} cm^{-3}, a radial average density of 4.9×10^{11} cm^{-3}, and an electron temperature of approximately 2 eV. Equation (12) would then predict an average ion saturation current density reaching the plasma grid of 9.9×10^{-3} A/cm^2. Since the grid apertures cover 79 cm^2 with a transparency of 52%, the saturation extraction current should be 407 mA. This in excellent agreement with the experimentally determined value of 390 mA. Further, from Eq. (13), saturation should occur at approximately 17 kV, which is also supported by the data.

ACKNOWLEDGMENTS

We acknowledge the assistance, in the form of equipment and advice, of the Plasma Technology group of the Fusion Energy Division of Oak Ridge National Laboratory, especially W. L. Stirling and H. H. Haselton. This research was supported by the Air Force Office of Scientific Research, Contract 80-0029. P. D. Weber is supported under appointment to the Magnetic Fusion Energy Technology Fellowship program which is administered for the U.S. Department of Energy by Oak Ridge Associated Universities.

REFERENCES

1. R. C. Davis, T. C. Jernigan, O. B. Morgan, D. L. Stewart, and W. L. Stirling, *Rev. Sci. Instrum.* 46, 576 (1975).
2. W. L. Stirling, C. C. Tsai, and P. M. Ryan, *Rev. Sci. Instrum.* 48, 533 (1977).
3. C. C. Tsai, W. L. Stirling, and P. M. Ryan, *Rev. Sci. Instrum.* 48, 651 (1977).
4. H. Horiike, M. Akiba, Y. Arakawa, S. Matsuda, and J. Sakuraba, *Rev. Sci. Instrum.* 52, 567 (1980).
5. C. Lejeune, *Nucl. Instrum. Methods* 16, 429 (1974).
6. C. Lejeune, J. P. Grandchamp, J. P. Gilles, and J. Aubert, *IEEE Trans. Nucl. Sci.* 23, 1084 (1976).
7. C. Lejeune, J. P. Grandchamp, and J. Aubert, *Rev. Phys. Appl.* 12, 1835 (1977).
8. R. Keller and H. Winter, *Part. Accel.* 7, 77 (1976).
9. O. Okada, private communication, Hitachi Corp.
10. M. D. Nahemow, Conference Record of the IEEE Int. Conf. on Plasma Science, San Diego, California, 1983, IEEE Cat. No. 83CH1847-3.
11. S. C. Brown, in *Basic Data of Plasma Physics*, M.I.T. Press, Cambridge (1967), p. 143.
12. C. Lejeune, Ph.D. thesis, Orsay, France (1971).
13. H. Winter and B. H. Wolf, *Plasma Phys.* 16, 791 (1974).
14. I. Langmuir, Phys. Rev. 33, 954 (1929).
15. R. A. Jacobsen and H. P. Eubank, *Plasma Phys.* 15, 243 (1973).
16. C. Lejeune, in *Applied Charged Particle Optics*, A. Septier, ed., Academic Press, New York (1983), pp. 207–227.
17. D. Bohm, in *Electric Discharges in Magnetic Fields*, A. Guthrie and R. K. Wakerling, eds., McGraw-Hill, New York (1949), pp. 77–86.
18. P. D. Prewett and J. D. Allen, *Proc. Phys. Soc. London, Sec. A* 348, 435 (1976).
19. K. Uehara, K. Yatsu, S. Hagiwara, and S. Kojima, *Jpn. J. Appl. Phys.* 14, 1761 (1975).